Comparative assessment of control strategies for the biradial turbine in the Mutriku OWC plant

François-Xavier Faÿ [a, b, *], João C. Henriques [c], James Kelly [d], Markus Mueller [e], Moahammad Abusara [e], Wanan Sheng [f], Marga Marcos [b]

[a] TECNALIA. Energy and Environment Division, Parque Tecnológico de Bizkaia, 48160, Derio, Bizkaia, Spain
[b] DISA, Univ. of the Basque Country UPV/EHU, Bilbao, Spain
[c] LAETA, IDMEC, Instituto Superior Técnico, Universidade de Lisboa, Av. Rovisco Pais, 1049-001, Lisboa, Portugal
[d] MaREI Centre, Beaufort Building, Environmental Research Institute, University College Cork, Ringaskiddy, Co. Cork, Ireland
[e] Renewable Energy, University of Exeter Penryn Campus, Treliever Road, Penryn, Cornwall, TR10 9EZ, United Kingdom
[f] SW Mare Marine Technology, Ireland

ARTICLE INFO

ABSTRACT

To be competitive against other renewable energy sources, energy converted from the ocean waves needs to reduce its associated levelised cost of energy. It has been proven that advanced control algorithms can increase power production and device reliability. They act throughout the power conversion chain, from the hydrodynamics of wave absorption to the power take-off to improve the energy yield. The present work highlights the development and test of several algorithms to control the biradial turbine which is to be installed in the Mutriku oscillating water column plant. A collection of adaptive and predictive controllers is explored and both turbine speed controllers and latching strategies are examined. A Wave-to-Wire model of one chamber of the plant is detailed and simulation results of six control laws are obtained. The controllers are then validated using an electrical test infrastructure to prepare the future deployment in the plant. Finally, the control strategies are assessed against criteria like energy production, power quality or reliability.

1. Introduction

In a global context of climate change, Nations are getting organised to limit and reduce their emission of greenhouse gas. The Paris Climate Agreement signed by 183 countries, representing 90% of the emissions, announced their will to politically engage in planning for a low carbon strategy. Pursuing the development of clean and renewable energy is clearly in line with this agreement. There is a tremendous amount of energy available worldwide from clean sources. The members of the European Union are on track to reach the objective of 20% of renewable production in 2020 [1]. The renewable energy sector is a fast growing industry especially coming from conventional sources where technologies are now mature. Wind, solar, and hydropower plants represent 90% of the installed renewable capacity in the European Union in 2017 [2]. The past decade has seen a drop of the cost of renewable energy such that they started competing with other type of conventional electricity generation. Recently some offshore wind farms to be developed in the North sea were granted without subsidies.

Technology developers and policy makers are convinced that energy converted from the oceans can follow the same path and consolidate the renewable energy mix by relying on an energy widely available and more predictable. The wave energy sector is still at an early development phase as can attest the wide diversity of concepts [3—6] and as many means of power extraction via the Power Take-Off (PTO) [7—10]. Plus there is not a clear sign of technology convergence that is also an evidence of the low maturity of the sector. The lack of confidence slows down private investments because of the risk associated. Also, as every early technologies, the cost of energy is for now too high. This is a breeding ground for innovation to foster the development of efficient technologies.

In wave energy conversion, among the many existing concepts, the Oscillating Water Column (OWC) type is one of the simplest. It uses the pneumatic power trapped inside an air chamber and

* Corresponding author. TECNALIA. Energy and Environment Division, Parque Tecnológico de Bizkaia, 48160, Derio, Bizkaia, Spain.
E-mail address: francois-xavier.fay@tecnalia.com (F.-X. Faÿ).

Nomenclature

Romans

a	generator control law constant
A_∞	limiting value at infinite frequency of the added mass, [kg]
$A(\omega_j)$	wave amplitude as function of the wave frequency, [m]
B	magnetic field in the air gap, [T]
b	generator control law exponent
d_{ip}	thickness of the iron core steel plate, [mm]
d_t	turbine rotor diameter, [m]
f_o	frequency of occurrence of a sea state, [%]
f_{hz}	generator frequency, [Hz]
F_{exc}	excitation force on the IWS, [N]
F_{rad}	radiation force of the IWS, [N]
F_h	hydrostatic force of the IWS, [N]
F_{press}	pressure force of the IWS, [N]
g	acceleration of gravity, [m/s^2]
h_{ch}	air chamber height at mean tide, [m]
H_s	significant wave height, [m]
I	turbine/generator set moment, [kg m^2]
$\mathbf{I}_r$	radiation state, [−]
I_{RMS}	stator RMS current, [A]
K	radiation impulse function, [N/m]
l_{ch}	air chamber length, [m]
m	mass of the rigid piston, [kg]
m_c	mass of air inside the chamber, [kg]
$\dot{m}_t$	turbine mass flow rate, [kg/s]
M_{mn}	ratio of maximal over nominal torque, [−]
N_{pp}	number of generator pair of poles, [−]
p	absolute air chamber pressure, [Pa]
p^*	dimensionless relative pressure, [−]
p_{at}	absolute atmospheric pressure, [Pa]
P_g	generator electrical power, [W]
P_{il}	generator iron power losses, [W]
P_{ml}	generator mechanical power losses, [W]
P_t	turbine aerodynamic power, [W]
P_{wl}	generator winding power losses wave-crest length, [W]
R_{st}	generator stator resistance, [Ohm]
S_{IWS}	OWC water plane area, [m^2]
t	time, [s]
T_0	IWS first resonant period, [s]
T_{ctrl}	torque control, [Nm]
T_e	energy period, [s]
T_g	generator torque, [Nm]
T_{latch}	latching time for CL3, [s]
T_{loss}	test bench torque losses, [Nm]
T_t	turbine torque, [Nm]
u_v	safety valve control variable, [0/1]
V_0	volume of air inside the chamber in calm water, [m^3]
V_c	instantaneous air chamber volume, [m^3]
V_{nom}	nominal generator voltage, [V]

w_{ch}	air chamber width, [m]
w_{gen}	generator weight, [kg]
z	heave position, [m]

Greek symbols

γ	specific heats ratio of air, C_p/C_v, [−]
$\Gamma(\omega_j)$	excitation force per unit wave amplitude, [N/m]
η_t	turbine efficiency, [−]
η_g	generator efficiency, [−]
κ_{gb}	virtual gearbox, [−]
κ_i	virtual inertia, [−]
λ	Froude scaling factor, [−]
Π	turbine dimensionless power, [−]
ϱ_{at}	air density at atmospheric conditions, [kg/m^3]
ϱ_c	stagnation air density at turbine inlet, [kg/m^3]
ϱ_w	water density, [kg/m^3]
Φ	turbine dimensionless flow rate, [−]
ϕ	phase of IWS response, [rad]
φ	wave random phase, [0,2π]
Ψ	turbine dimensionless pressure head, [−]
ω	wave frequency, [rad/s]
Ω	turbine/generator set rotational speed, [rad/s]
Ω_{max}	generator maximal rotational speed, [rpm]
Ω_{nom}	generator nominal rotational speed, [rpm]
σ_e	eddy current loss coefficient, [−]
σ_h	hysteresis loss coefficient, [−]
Υ	Spectrum attenuation function, [−]

Superscripts

*	dimensionless quantity

Subscripts

at	atmospheric quantity
bep	best efficiency point
ch	chamber
g	generator quantity
in	turbine inlet conditions
iws	internal water surface
m	model scale
max	maximum value
nom	nominal value
p	prototype scale
r	test bench real scale
t	turbine quantity

Acronyms

CL	Control law
HIL	Hardware in-the-loop
IWS	Internal Water Surface
MWPP	Mutriku Wave Power Plant
OWC	Oscillating Water Column
PTO	Power Take-Off
RAO	Response Amplitude Operator
W2W	Wave-to-Wire model
WEC	Wave Energy Converter

created by the oscillating movement of the waves to drive an air turbine. This turbine is then connected to a conventional generator to produce electricity. State of the art publications are available in Refs. [11–14]. Actually several concepts using this technology have reached sea trials. Both fixed and floating structures were deployed at sea, just to name some of them: the Mighty Whale in Japan, the Pico plant in Azores Islands [15], the Limpet in the Island of Isle, the bottom standing OWC of Trivandrum India, the Backward Bent Duct Buoy from Ocean Energy, the Oceanlinx nearshore OWC, the bottom-standing plant at Yongsoo in South Korea, the Mutriku Wave Power plant and the Marmok-A5 from Oceantec/IDOM in the north of Spain.

The area of control in wave energy is acting to optimise the energy production, inducing more incomes, while requiring little additional investments, and is identified to be one of the key cost-reduction pathways to reduce the cost of energy [16]. Extensive work on control theory applied to the wave energy conversion has been produced [17–20]. Optimum control theory goal is to perform a phase and amplitude matching so the Wave Energy Converter (WEC) enters in resonance condition, amplify its motion and absorb more power. Two main types of phase control exist: reactive control [21–23] and latching control [24–26]. Reactive control relies on a PTO capable of sending back energy to the system to change its motion, whereas latching requires a mechanism to keep the WEC motion still and release it at the right moment. Some of them are relying on Model Predictive Control algorithms [27–29] to further improve their performance. However, these strategies were criticised first of all theoretically because the linear potential flow theory assumptions do not apply anymore [18,30], and in the issues of real implementation. The absence of latching mechanisms robust enough [31], or in reactive control the double generator efficiency penalisation of the power flowing from the PTO to the float absorber [32], and also in the need for predicting the wave force [25,33]. Few were actually tested experimentally [34,35] and even less had the opportunity to be deployed in real sea environment [36].

For the case of the OWC, the main type of control strategy employed is called turbine speed control. It consists in adjusting the turbine speed by applying a generator torque in order to set the turbine at good efficiency ranges [37–40] and, in the case of the Wells, avoid stalling events, sometimes supported by airflow control [41,42]. Theoretical studies were performed on latching in Refs. [43–47]; and experimental work is done on a small scale sparbuoy in Ref. [48]. Electrical test infrastructures were used for the speed controls in Refs. [49–52] to validate the implementation of algorithms in Hardware-in-the-Loop (HIL) experiments. Real sea testing of devices and control using OWC systems are reported in Refs. [53–56].

The focus of this work is to develop, assess and compare the performance of several control strategies applied to the OWC. Along the European Union funded project H2020 OPERA project, these controllers will be implemented first in the Mutriku plant and then to the Marmok-A5 from Oceantec/IDOM. Numerical simulations are done using the same Wave-to-Wire model (W2W) that describes one of the 16 chambers composing the OWC plant in Mutriku. These algorithms act throughout the power conversion chain; from the hydrodynamics of wave absorption to the turbine aerodynamic and electrical equipment efficiency. After numerical simulations, all the algorithms are validated for deployment with dry testing in one of the two available test facilities. In total, 6 control laws (CL) are presented (c.f. Table 1), and composed of adaptive controllers and a predictive one. The adaptive controllers are based on operational plant data to define the instantaneous control action, and the predictive strategy performs an online optimisation during a prediction horizon. Also, despite the adaptive/predictive distinction, two types of control strategies are

classified; turbine speed controllers act to set the Power Take-Off (PTO) to its best point of efficiency, and the latching control strategies aiming at modifying the WEC motion in order to force resonant conditions with the incident waves. Latching is made possible here by the fast actuating HSSV installed at the inlet of the turbine rotor.

The paper is structured in six main parts. Section 2 describes the Mutriku Wave Power Plant (MWPP), starting with the available water resource and the motion of the internal water surface for one of the 16 chambers of the plant. Then, the air chamber dynamics and the interaction with the biradial turbine are explained as well as the power conversion components. The derived W2W time domain numerical model will be used as the common framework for all the controllers. Section 3 consists in the description of the 6 control laws, detailing their requirements. The results assessment is done in Section 4 which describes all the numerical simulations process and the results to ease the comparison of the different control laws, while Section 5 addresses the laboratory tests. First, the two facilities used to conduct them are described, followed by the explanation of the tests carried out and the results obtained. Finally, Section 6 concludes the paper.

2. Mutriku power plant wave-to-wire model

The Mutriku wave energy plant is built inside the new harbour breakwater in the Bay of Biscay [57,58]. The technology selected for the energy conversion is the OWC. A common framework is required for the comparison of the control algorithms. Thus, a time domain numerical model of one of the air chambers along with its PTO system are developed and will be used as the common basis for all the controllers. The frequency domain study detailing the computation of the plant's hydrodynamic coefficients can be found [40,59]. The plant physical parameters and the chamber dimensions are shown in Table 2.

2.1. Wave resource

Although the Mutriku plant produces energy in its local wave climate, the plant operation was designed using only 14 distinct sea states (SS) according to the site-specific occurring incident sea

Table 2
Characteristics of the Mutriku power plant.

Parameters	Symbol	Value	Unit
Pysical quantities			
Water density	ρ_w	1025	kg/m^3
Atmospheric air density	ρ_{at}	1.25	kg/m^3
Gravitational constant	g	9.81	m/s^2
Atmospheric pressure	p_{at}	101.5	kPa
Air specific heats ratio	γ	1.40	–
Plant dimensions			
Chamber width	w_{ch}	4.50	m
Chamber length	l_{ch}	3.10	m
Chamber height (mean tide level)	h_{ch}	7.45	m

Table 1
Summary of control laws.

Control Law	Adaptive/Predictive	Controls	Based on
CL1	Adaptive	Generator torque	Rotational speed
CL2	Adaptive	Generator torque	Chamber pressure
CL3	Adaptive	Valve open-close timings	Hourly sea state, chamber pressure
CL4	Adaptive	Valve open-close timings	Chamber pressure, valve position
CL5	Adaptive	Generator torque	Rotational speed
CL6	Predictive	Generator torque	One period future wave elevation, Rotational speed

states [57]. The characteristics sea states are presented in Table 3 with respect to their significant wave height H_s, the energy period T_e and the frequency of occurrence f_0.

The wave power plant is situated in shallow waters, hosted in a breakwater so it would be incorrect to assume a typical wave spectrum to that used in offshore applications. To take into account the effect of finite depth in front of the plant, a TMA spectrum approach [60] is used to model the waves motion. A site-specific attenuation function was applied as shown in Appendix A.

2.2. Internal water surface motion

The heave motion $z(t)$ of the Internal Water Surface (IWS) was modelled as an imaginary rigid piston of mass m. This approximation is expected to be accurate since the characteristic dimension of the air chamber is much smaller than the wave length. Based on the Newton's 2nd law, the equation of motion is

$$(m + A_\infty)\ddot{z}(t) = F_{exc}(t) + F_{rad}(t) + F_h(t) + F_{press}(t). \tag{1}$$

Here A_∞ denotes the added mass when the frequency tends to infinity.

The excitation force F_{exc} is the force of an incoming wave upon the IWS

$$F_{exc}(t) = \sum_{j=1}^{N} \Gamma(\omega_j)\, A(\omega_j)\sin(\omega_j t + \phi(\omega_j) + \varphi_j), \tag{2}$$

with $\Gamma(\omega_j)$ the excitation force response per unit of wave amplitude A over the angular frequencies ω_j, obtained with the hydrodynamic solver WAMiT. The computation of the wave amplitudes is described in Appendix A. The phase response of the IWS with respect to the wave elevation, as function of ω_j, is denoted as $\phi(\omega_j)$, and φ_j are the wave random phases.

The wave radiation damping force F_{rad} in the time domain is computed by the convolution integral

$$F_{rad}(t) = -\int_0^t K(t-\tau)\,\dot{z}(\tau)\,d\tau. \tag{3}$$

Here K is the radiation impulse response function. In the present work, the radiation force is approximated using a 20th order Prony's method [61].

The hydrostatic restoring force is defined by

$$F_h(t) = -\rho_w g S_{iws}\, z(t), \tag{4}$$

where S_{iws} is the area of the IWS and ρ_w is the sea water density.

Table 3
Mutriku sea states.

SS	H_s [m]	T_e [s]	f_0 %
1	0.88	5.5	3.23
2	1.03	6.5	3.44
3	1.04	7.5	5.08
4	1.02	8.5	6.11
5	1.08	9.5	10.73
6	1.19	10.5	9.31
7	1.29	11.5	9.52
8	1.48	12.5	7.42
9	1.81	13.5	2.75
10	2.07	14.5	2.96
11	2.59	15.5	1.34
12	2.88	16.5	0.40
13	3.16	11.5	0.27
14	3.2	12.5	0.42
		Total	62.98

The resultant of the pressure forces, often called PTO force, in the internal water free surface is

$$F_{press} = -p(t)\, S_{iws}, \tag{5}$$

where $p(t)$ is the pressure in the chamber relative to the atmosphere.

Finally, the validation of the IWS motion is made by comparing the RAO obtained from the hydrodynamic study and running the time domain model in regular waves (c.f. Fig. 1). The relative error of the time domain model simulation with respect to the frequency-domain is also depicted.

2.3. Air chamber and PTO

2.3.1. Air compressibility model

Assuming a isentropic compression/expansion of air in the chamber, the following relation can be stated

$$\frac{p + p_{at}}{\rho_c^\gamma} = \frac{p_{at}}{\rho_{at}^\gamma}, \tag{6}$$

where ρ_c is the air density inside the chamber, and γ is the specific heats ratio for air. The subscript "at" denotes atmospheric conditions. Introducing the dimensionless relative pressure $p^* = p/p_{at} - 1$ and taking the derivative in time of Eq. (6), we obtain

$$\frac{\dot{\rho}_c}{\rho_c} = \frac{p^*}{\gamma(p^* + 1)}. \tag{7}$$

The mass balance in the air chamber is given by

$$\frac{d(\rho_c V)}{dt} = -\dot{m}_t, \tag{8}$$

or

$$\frac{\dot{V}_c}{V_c} + \frac{\dot{\rho}_c}{\rho_c} = -\frac{\dot{m}_t}{m_c}, \tag{9}$$

where $V_c = S_{iws}(h_{ch} + z)$ is the instantaneous volume of the chamber, $m_c = \rho_c V_c$ denotes the mass of air inside the chamber, and $\dot{m}_t$ is the turbine flow rate (positive for exhalation). Replacing Eq. (6) in Eq. (9) gives
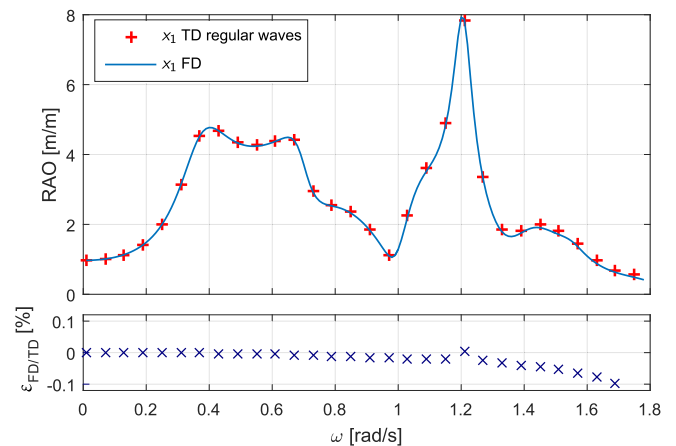

Fig. 1. Comparison of the RAO of the IWS motion obtained from the time domain model using Prony method and the frequency domain one.

$$\frac{p^*}{p^* + 1} = - \gamma \left(\frac{\dot{V}_c}{V_c} + \frac{\dot{m}_t}{m_c} \right). \tag{10}$$

To solve Eq. (10) in time, the density ρ_c is computed using Eq. (6). The computation of the turbine mass flow rate is described in the next section.

2.3.2. Biradial turbine

The biradial turbine is a novel turbine whose air flow enters the stator and exits the diffuser radially. It has been design and manufactured in the framework of the OPERA project and the turbine behaviour and performance are shown in Fig. 2 were obtained during the design phase. The characteristics can be represented with the dimensionless coefficients of pressure head Ψ, mass flow rate Φ, turbine power Π, and efficiency η_t as

$$\Psi = u_v \frac{p}{\rho_{in} \Omega^2 d_t^2}, \tag{11}$$

$$\Phi = \frac{\dot{m}_t}{\rho_{in} \Omega d_t^3}, \tag{12}$$

$$\Pi = \frac{P_t}{\rho_{in} \Omega^3 d_t^5}, \tag{13}$$

$$\eta_t = \frac{\Pi}{\Psi \Phi}. \tag{14}$$

Here ρ_{in} denotes the air density at inlet stagnation conditions, Ω is the turbine rotational speed, d_t is the turbine rotor diameter, and P_t is the turbine aerodynamic shaft power. u_v denotes the valve actuation and its control sequence is described in the following section. In the inhalation half cycle, $\rho_{in} = \rho_{at}$. For the exhalation half cycle, $\rho_{in} = \rho_c$. In the current work, we made the approximation that $\rho_{in} \approx \rho_{at}$ which is reasonably valid for low energetic sea states. The turbine has a rotor diameter of $d_t = 0.5$ m.

2.3.3. High-speed stop valve

The turbine is equipped with the high-speed stop valve (HSSV) installed in series with the turbine that controls the flow rate. The fast actuation, around 1/5 s, enables the use of latching control

strategies. Also, it can be operated to avoid overspeeding the turbine/generator set. There is a risk of failure if the maximum speed is exceeded due to the increase of mechanical vibrations and centrifugal forces. The valve position (closed-0, or open-1) is determined by the associated control variable u_v and its control is common for all the CL.

$$u_v = \begin{cases} 0, & \text{if } u_v = 1 \text{ and } \Omega > \Omega_{th,up}, \\ 0, & \text{if } u_v = 0 \text{ and } \Omega > \Omega_{th,dn}, \\ 1, & \text{otherwise}. \end{cases} \tag{15}$$

The threshold speed are defined by the upper limit $\Omega_{th,up} = 3000$ rpm to close the valve and the $\Omega_{th,dn} = 2500$ rpm to open it.

2.3.4. Electrical conversion

An asynchronous induction generator is connected to the turbine shaft and is responsible for converting the mechanical energy to electricity. Its specifications are collected in Table 4.

The generator loss model includes the main losses that affect the conversion from mechanical to electrical power that are:

- mechanical losses P_{ml},
- iron losses P_{il},
- winding losses P_{wl}.

The bearings mainly cause mechanical losses. Its value can be estimated as a function of the shaft diameter and the rated power for a type of generator (number of poles). Fig. 3 shows the estimation of these losses with data extracted from Ref. [62].

Iron losses are due to iron core perturbation on the magnetic field and can be calculated as seen in Ref. [63] following

$$P_{il} = B^2 \left(\sigma_h \frac{f_{hz}}{100} + \sigma_e \left(\frac{d_{ip} f_{hz}}{100} \right)^2 \right) w_{gen}, \tag{16}$$

where the average magnetic field in the air gap is set to $B = 0.8$ T. The hysteresis and eddy current loss coefficients have been selected to be respectively $\sigma_h = 5.01$ and $\sigma_e = 44.80$ and come from an adjustment made on the generator presented in Ref. [64]. The iron core steel plate thickness is selected to be $d_{ip} = 0.64$ mm given in Ref. [65].

Finally the winding losses are derived from the RMS stator current and the stator resistance R_{st} following this equation

$$P_{wl} = I_{rms}^2 R_{st}. \tag{17}$$

The generator electrical power is then computed with the sum of the loss resting to the turbine power so that
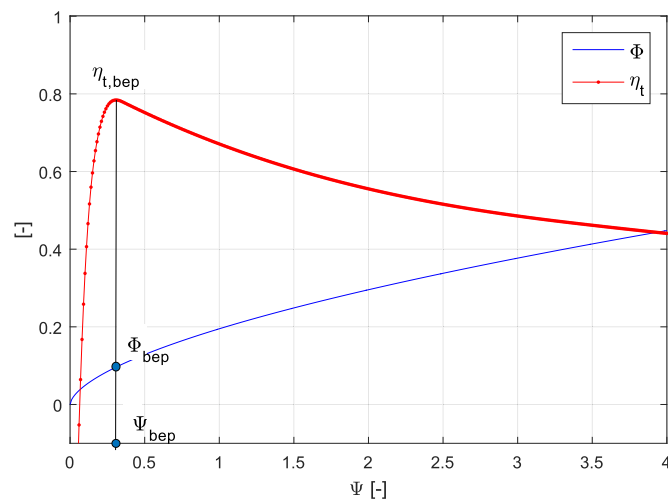

Fig. 2. Biradial turbine characteristic curves computed in the design phase. The values corresponding to the best efficiency points are also plotted.

Table 4
Generator specifications.

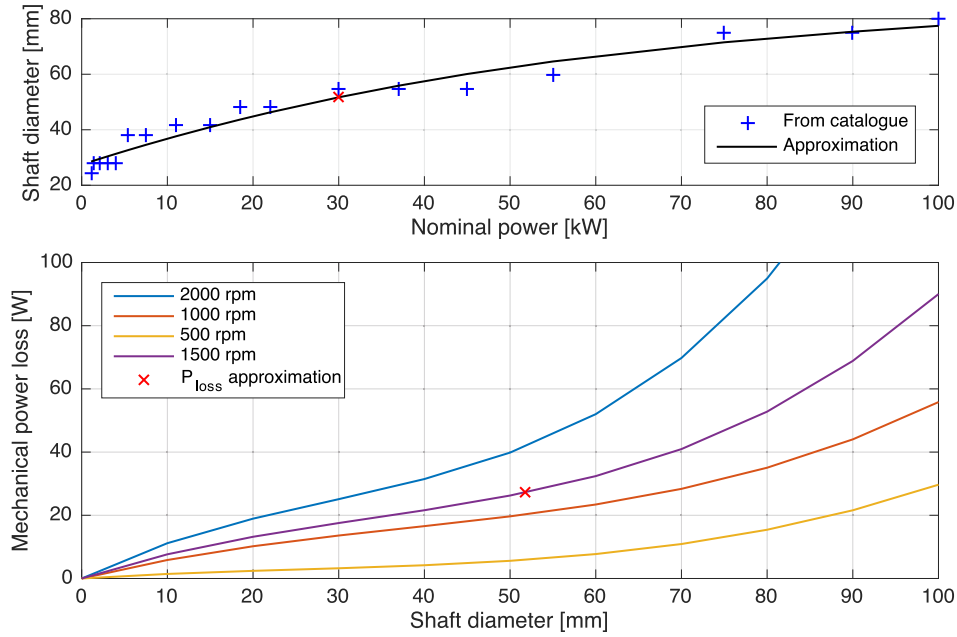| Parameters	Symbol	Value	Unit
Nominal power	$P_{g,nom}$	30	kW
Nominal torque	$T_{g,nom}$	190	Nm
Nominal speed	Ω_{nom}	1500	rpm
Pairs of Poles	N_{pp}	2	—
Max/Nom torque ratio	M_{mn}	2	—
Runaway speed	Ω_{max}	4500	rpm
Insulation class	—	Class H (180 °C)	—
Weight	w_{gen}	250	kg
Nominal voltage	V_{nom}	400	V
Frequency	f_{hz}	50	Hz

Fig. 3. Estimation of the generator mechanical losses.

$$P_g = P_t - (P_{ml} + P_{il} + P_{wl}), \tag{18}$$

and its efficiency is the ratio $\eta_g = P_g/P_t$.

2.3.5. Generator operational regions

Due to the intrinsic nature of wave energy, the generator will have to be operated over its nominal condition and deal with peaks of production during short periods of time. The operational limitation of an induction generator is defined by its current and voltage limits. Below the nominal voltage in the constant torque region, the current limit is proportional to the maximum torque. It is possible to operate a generator at maximum current periodically keeping in mind that the temperature of the windings will rise and cannot reach a certain threshold. Over the rated voltage the generator enters the flux-weakening operation region. The maximum electrical torque decreases with the square of the speed due to the magnetic forces in the generator whereas the mechanical load torque decreases with the inverse of the speed and the nominal power is then constant. The different operation regimes are presented in Fig. 4. In the current configuration, the generator's 3 phases are connected to a frequency converter which rated voltage is $V_{PE,nom} = 690V$ and sized 3 times higher than the generator power. This configuration allows an overspeed of the generator and shifts the voltage limit to the overspeed threshold:

$$\Omega_{os} = \frac{V_{PE,nom}}{V_{nom}} \Omega_{nom} \tag{19}$$

The maximal peak power over that configuration is thus $P_{max} = M_{mn} T_{g,nom} \Omega_{os} \approx 100$kW.

2.3.6. Drive train implementation

The dynamics of the drive train of inertia I describing the turbine/generator set angular acceleration is given by

$$I\dot{\Omega} = T_t - T_g, \tag{20}$$

where $T_g = P_g/\Omega$ is the generator electromagnetic torque.

3. Control laws description

All the adaptive and predictive control laws are explained here, including the speed controllers and the latching strategies.

3.1. CL1: torque control based on turbine speed

The first CL is based on several research papers [37,51,66] and adapted for the case of the Mutriku plant. The controlled torque to be applied by the generator is related to the fact that along with a time frame long enough the average of the turbine and generator powers are equal considering a lossless drivetrain.

A simple and effective generator control can be derived from the turbine power using simple physical arguments. If the goal is to maximise the turbine efficiency then the turbine is to be operated at the best efficiency point Ψ_{bep}, see Fig. 2, and the turbine power is computed from Eq. (13) as

$$P_t\left(\Psi_{bep}, \Omega\right) = \varrho_{at}\, d_t^5\, \Pi\left(\Psi_{bep}\right)\Omega^3 = \text{const } \Omega^3. \tag{21}$$

As such, the generator power control could follow a relation of the type

$$T_{ctrl} = a\, \Omega^b, \tag{22}$$

where the exponent b should be around 2.

An offline optimisation is used to tune the slope a and b exponent coefficients of the torque law and parametrise the control parameters for the MWPP. Besides, a peak power control is included to limit the reference control torque and avoid overloading the generator. The CL used in the numerical simulations is then
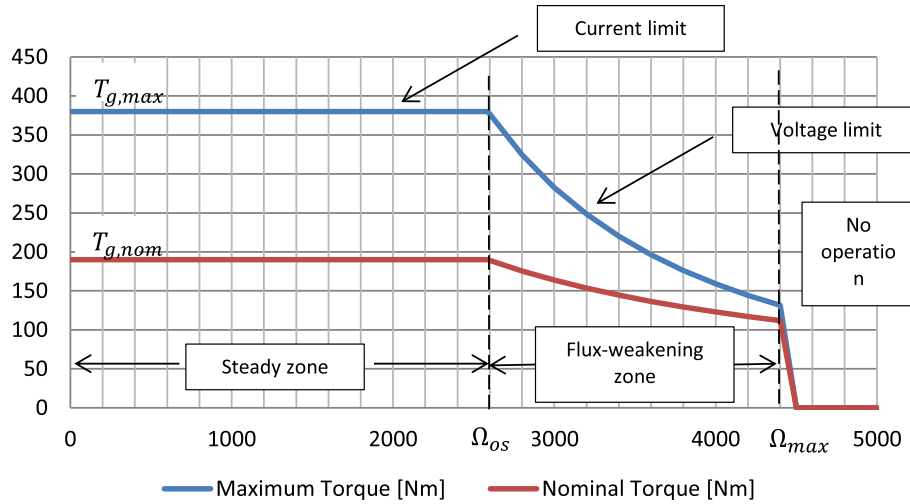
Fig. 4. Generator possible operations regions.

$$T_{\text{ctrl}} = \min\left(a\,\Omega^b, P_{\text{g,nom}}\,/\,\Omega\right). \tag{23}$$

3.2. CL2: torque control based on chamber pressure

The second control algorithm developed in this study uses a torque law not based on the instantaneous rotational speed but on the relative chamber pressure. It arises from work performed in Ref. [54]. The derived controlled torque yields to the generator torque law:

$$T_{\text{ctrl}} = k_0 + k_1 \bar{p}, \tag{24}$$

with the constants k_0 and k_1 determined by numerical evaluations of the biradial turbine characteristics. The 5-min average of the absolute value of the relative chamber pressure $\bar{p}$ is introduced, replacing the instantaneous pressure drop. Indeed the sudden changes in internal pressure would yield to hazardous change of the controlled torque resulting in stressing the generator. The length of the moving average window was determined to allow a responsive evolution of the generator torque.

An overspeed protection feature is introducing to operate the turbine safely and avoid overspeeding in high energetic seas. A third term was added to Eq. (24), responsible for increasing the controlled torque in instantaneous high-pressure values and brake down the turbine. Finally, CL2 torque law is:

$$T_{\text{ctrl}} = k_0 + k_1\,\bar{p} + k_2\,|p - \bar{p}|. \tag{25}$$

3.3. CL3: latching control based on sea state data

This control law is a modified latching control from Refs. [67,68], but the control law does not require precise future wave prediction. Instead, the control law will use the wave energy period T_e from previous wave forecast statistics. Therefore, this control law is proposed as a sub-optimal control for improving wave energy conversion for the OWC devices.

The implementation of the control law includes the closing and opening of the control valve. The latching durations are calculated based on the sea state and the internal water surface first resonance

period T_0. The physical implementation of the control law is as following.

- Step 1 - The control law closes the HSSV when the chamber relative pressure p is around zero.
- Step 2 - The valve stays closed during the latching duration and then goes back to the open position

$$T_{\text{latch}} = \frac{T_e - T_0}{2}. \tag{26}$$

3.4. CL4: Threshold latching based on turbine speed and chamber pressure

The CL4 is an enhanced version of the strategy 2 described in Refs. [43,44] and it is called in the literature as threshold latching. It uses the rotational speed and the air chamber pressure to control the HSSV position. The main goal is to avoid over-powering the turbine and the generator in more energetic sea states. The variable used to compute the opening instants is the pressure head coefficient Ψ.

The latching control implemented within this control, is based on a positive threshold for the pressure head coefficient, Ψ_{thr}^+, and a negative threshold, Ψ_{thr}^-. When Ψ is positive and is above Ψ_{thr}^+ then the valve is opened. The valve is closed when $\Psi < \Psi_{\text{thr}}^+$ and the elapsed time after the opening order is greater than a specified time interval Δt_{min}. Analogous strategy is applied when Ψ is negative. The threshold values Ψ_{thr}^+ and Ψ_{thr}^- are to be determined experimentally. The used of a pre-defined minimum elapsed time Δt_{min} after the opening order aims to avoid intermittent operation for short time intervals. The outer-loop of this control law applies the generator control law CL1 as given by Eq. (23).

3.5. CL5: torque control based on reinforcement learning

CL5 is an application of Reinforcement Learning for the control of the biradial turbine in the Mutriku power plant. The goal is to find the optimal curve relating the maximum power and turbine rotational speed, by measuring the output generator power and adjusting the generator torque accordingly. A model-free control was adopted to perform an on-line optimisation with operational data. The main aim is to tune the coefficient a of the torque law Eq.

(22)) without relying on the plant model. This approach makes CL5 unbiased by modelling errors or changes in the model due to "wear and tear".

In general Reinforcement Learning, an agent, which is in a particular state s_n, interacts with the surrounding environment by taking an action a_n, where n defines the time step of the algorithm. The agent then moves to a new state, s_{n+1}, and the action is followed by a reward, r_{n+1}, depending on its outcome. The action selection process is modelled as a Markov decision process based on the value function that defines the estimate of the future reward. The agent is expected to learn optimal behaviour over time for the maximisation of the total reward [69].

The implementation presented here applies a Q-Learning algorithm. The state variables are chosen to be a 2-dimensional discretisation of the turbine speed and generator power

$$S = \left\{ s \middle| s_{jl} = \left(\Omega_j, P_{g,k} \right), j = 1, \ldots, J, l = 1, \ldots, L \right\}, \quad (27)$$

where J and L determine the number of states. The action a_n at any time n is chosen to be one of the following: i) increase, ii) decrease, or iii) do not change the generator torque (given the same turbine speed); or equivalently: i) increase, ii) decrease, or iii) do not change the slope coefficient a. Thus, we have an action space

$$A = \left\{ a \middle| a \in \left\{ -\Delta a, \ 0, \ +\Delta a \right\} \right\}. \quad (28)$$

The reward is chosen to be a function of the average (over a time-horizon, here few wave-lengths) output power as:

$$r_{n+1} = \begin{cases} \Delta P_{\text{avg},g,n+1}/1000, & \Delta P_{\text{avg},g,n+1} > \delta, \\ 0, & -\delta < P_{\text{avg},g,n+1} < \delta, \\ \Delta P_{\text{avg},g,n+1}/1000, & \Delta P_{\text{avg},g,n+1} < -\delta, \end{cases} \quad (29)$$

where δ is a design parameter (minimal viable change in average power) applicable to all sea states. Scaling the power by $1/1000$ for the reward function has proven to be more efficient in simulations in varying sea states.

The Reinforcement Learning algorithm employs an exploration strategy to find the optimum value of the slope coefficient a of the torque law Eq. (22), and thus the optimal torque. This is achieved by updating a Q-table as a function of reward and previously accumulated (but over time discounted) rewards for any state/action combination, and using the Q-table (thus previous rewards for taken actions at given states) together with an exploration rate, to decide the current action. Exploration rate, learning rate and discount factors are design parameters which are chosen to accommodate the trade-off between fast convergence of the exploration strategy and robustness of the result with respect to uncertain external conditions, i.e., varying sea states and model uncertainties.

3.6. CL6: predictive torque control based on future wave elevation

The following controller is a non-linear model predictive control using a receding horizon frame to perform the on-line optimisation. The aim is to maximise both the turbine and generator efficiency, so the power output is optimal for a fixed prediction horizon T_H as a function of the incoming waves. It is based on the torque law proposed in Eq. (22), which relies on a lossless drivetrain and the characterisation of the turbine, at the difference that the proposed strategy computes the instantaneous control torque accounting for the overall power conversion.

Two phases characterise this control law: i) the computation of the control coefficients a and b of Eq. (22) during the prediction horizon, and ii) their application during the replanning period.

During the prediction horizon, an on-line optimisation determines the best coefficients a and b of the torque law Eq. (22) and constitutes the control vector $\mathbf{u} = \begin{pmatrix} a & b \end{pmatrix}$. The newly characterised control law is then applied them during the re-planning time. The optimisation algorithm maximises the performance index

$$J(\mathbf{u}) = \frac{1}{T_H} \int_0^{T_H} \left(\alpha \, P_t + \beta \, P_g(\mathbf{u}) \right) \mathrm{d}t. \quad (30)$$

Note that the turbine power output is indirectly affected by the control vector $\mathbf{u}$. The parameters α and β are weighting parameters used to prioritise the power absorption or power conversion into electrical power.

4. Assessment of the control laws based on simulation results

This section highlights the performance of each control law in terms of power production, reliability and power quality. The simulation results are obtained for all the algorithms upon the 14 sea states presented in Table 3. CL1 is used as the base case control for comparing the algorithms. The time simulation of an individual test is set to 1/2 h to represent the typical time duration of a sea state. An exception is made for CL5 as it needs longer time simulation for the control parameters to converge. In this case a simulation of 12 h is set and the last 1/2 h is used for the analysis.

4.1. Power production

In Fig. 5, the energy production for each CL is defined as the sum of the energy produced during the 14 sea states (c.f. Table 3), including the frequency of occurrence and assuming the plant is available 100% of the time. The two latching control strategies, CL3 and CL4, show the lowest performance and their energy production is below the base case. The objective of a latching controller is to tune the device motion to obtain resonant condition and absorb more energy at the wave-structure interaction. Referring to Fig. 1, the RAO shows the plant always amplifies the wave motion (RAO > 1) so invalidating the use of such controllers for this plant. Instead of improving the performance, the two algorithms have a negative effect on the energy production due to an inappropriate use of the latching valve. CL2 presents a small increase in the energy produced with 4.4% of additional energy in respect to CL1. CL5 provides a substantial increase in respect to the base case (CL1) by producing
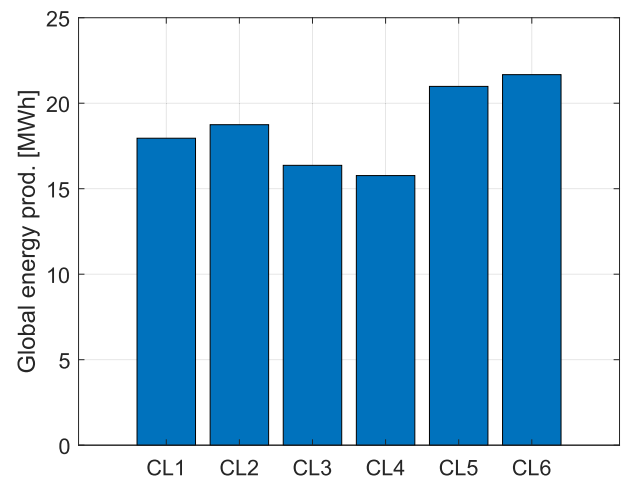

Fig. 5. Global energy production for each CL during the 14 sea states.

17% more energy. The predictive law CL6 outperforms all the CL by exerting an overall increase in energy production of more than 20% with respect to the base case.

The comparison of energy production against electrical power production is interesting in the sense that the overall energy produced includes the frequency of occurrence of the sea states which cannot be considered for the electrical power (c.f. the panels on the left-hand side of Fig. 6). It is relevant to analyse not only the efficiencies of the PTO subsystems but also the power produced at each energy conversion step for each CL and in a selection of SS as can be seen in Fig. 6: the results are detailed in terms of energy, powers (pneumatic, mechanical and electrical) and efficiencies (turbine, generator and overall PTO), for three distinct sea states corresponding to low, medium and high energetic wave conditions.

The control objective of CL1 is to reach the highest average turbine efficiency, around 70%, for all the sea states. The CL2 results show both poor turbine efficiency and poor generator efficiency. It makes up for the poor efficiencies with higher pneumatic power which is cause mostly by the extended availability of the PTO system. This shows up most prominently in the highest energy sea

states, where the CL2 produces the third most energy despite poor overall efficiency. The CL3 shows good turbine and generator efficiency, but it has less available pneumatic energy due to the latching of the air valve. Due to this loss of available pneumatic energy, the CL3 overall electrical energy output suffers and limits the effectiveness of CL3. CL6 is the one showing the best results in terms of energy for all the studied SS in comparison with the other CLs. The increase in SS5 and SS8 are around 10% and reaches 90% in the most energetic one. Focusing on the turbine efficiency, performance of CL6 is usually lower than the one of CL1 (around 5%) but on the other hand the generator operates at better regimes as its efficiency is around 10% higher. The overall PTO efficiency is thus close to 5% higher in CL6. As a general observation, the PTO efficiency when operating the predictive controller oscillates around 45–60%. Focusing on SS14, the pneumatic energy is almost twice as high as in CL1 and including the slight increase in efficiency one can understand the good score of this control strategy in terms of energy production. Mainly this can be explained by the inclusion of both the turbine and generator output power to the cost function. Also, in higher sea states, the predictive algorithm prevents the
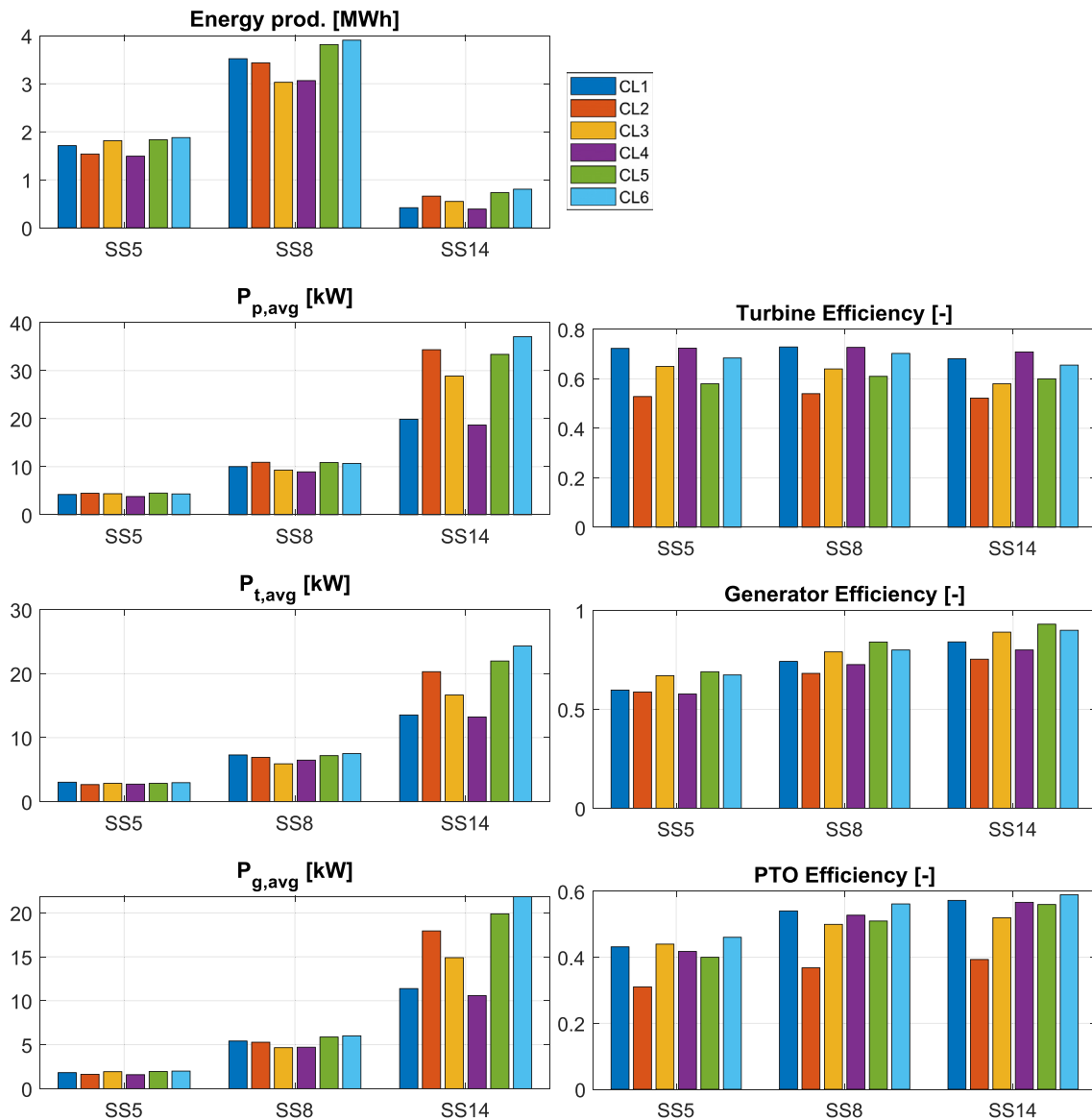

Fig. 6. Global performance of the 6 CL in SS5, SS8 and SS14.

HSSV from closing during long time duration, synonym of loss of absorbed energy, because it is capable of adapting the torque law parameters so that the turbine exceeds the cut-off speed less often. In general, the performance of a controller cannot be assessed only by its efficiency as it was highlighted that a less efficient CL could generate more output power (c.f. results for CL2).

Fig. 7 shows a detailed view of the turbine performance for all the control laws in SS8. On each panel, the probability distribution of the dimensionless pressure head Ψ is plotted together with the turbine efficiency. The more the pressure is distributed in the high turbine efficiency range the better the turbine performance. The two latching laws, CL3 and CL4, are quite recognizable with the highest probability appearing close to $\Psi = 0$. The latching valve is often closed, and thus the Eq. (11) yields to zero. For example, CL1 concentrates 87% of the dimensionless pressure probability in the range $\Psi = [-0.75 : +0.75]$, that refers to highly efficient operation regime of the turbine. CL6 concentrates 72% of the probability inside the same range, which classifies it just behind CL1 and CL4. On the other hand, a rather wide and even spread of dimensionless pressure probability can be observed for CL5, which is an indication that the learning algorithm is not controlling for optimal turbine efficiency but maximum long-term energy yield, and thus optimal generator efficiency (c.f. Fig. 8).

In Fig. 8 the CLs are evaluated in terms of generator performance operating under SS10, where the generator efficiency is plotted as a function of the generator load, $\Lambda = P_g/P_{g,\text{nom}}$. The first observation to be made refers to the type of controller employed. While CL1, CL3, CL4 and CL5 follow a unique trend line, CL2 and CL6 show a different pattern. The first case is very specific of a torque law and it can be seen that CL1 and CL4 use the same coefficients. CL3 and above all CL5 present higher efficiency scores compared to CL1 and CL4. The case of CL6 is particular because it is based on a torque law like most of the controllers but able to take not only the trend of CL1, for example, but as many as the optimisation can produce. This is an evidence of its capacity to adapt dynamically to internal and
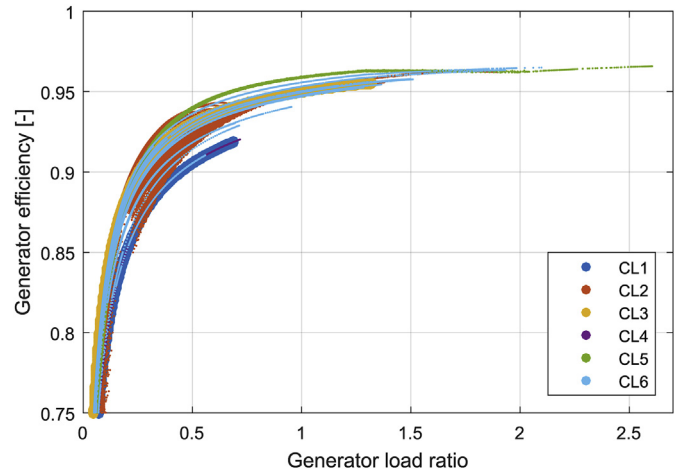

Fig. 8. Generator efficiency in function of the load.

external conditions. Because CL2 is not based on rotational speed but on pressure, it produces a curve shape that is very different to the other CLs with an efficiency clustered in the upper left part of the figure.

4.2. Reliability

This section analyses reliability issues, or how the different controllers do apprehend the components operation in extreme conditions. Quantities like the peaks in the generator production and valve operation are studied to understand how the different control laws deal with the operation above the nominal conditions. In Fig. 9 the probability distribution of the generator power is plotted for each CL during operation in the highest energetic sea state. The torque laws employed in CL1 and CL4 avoid any
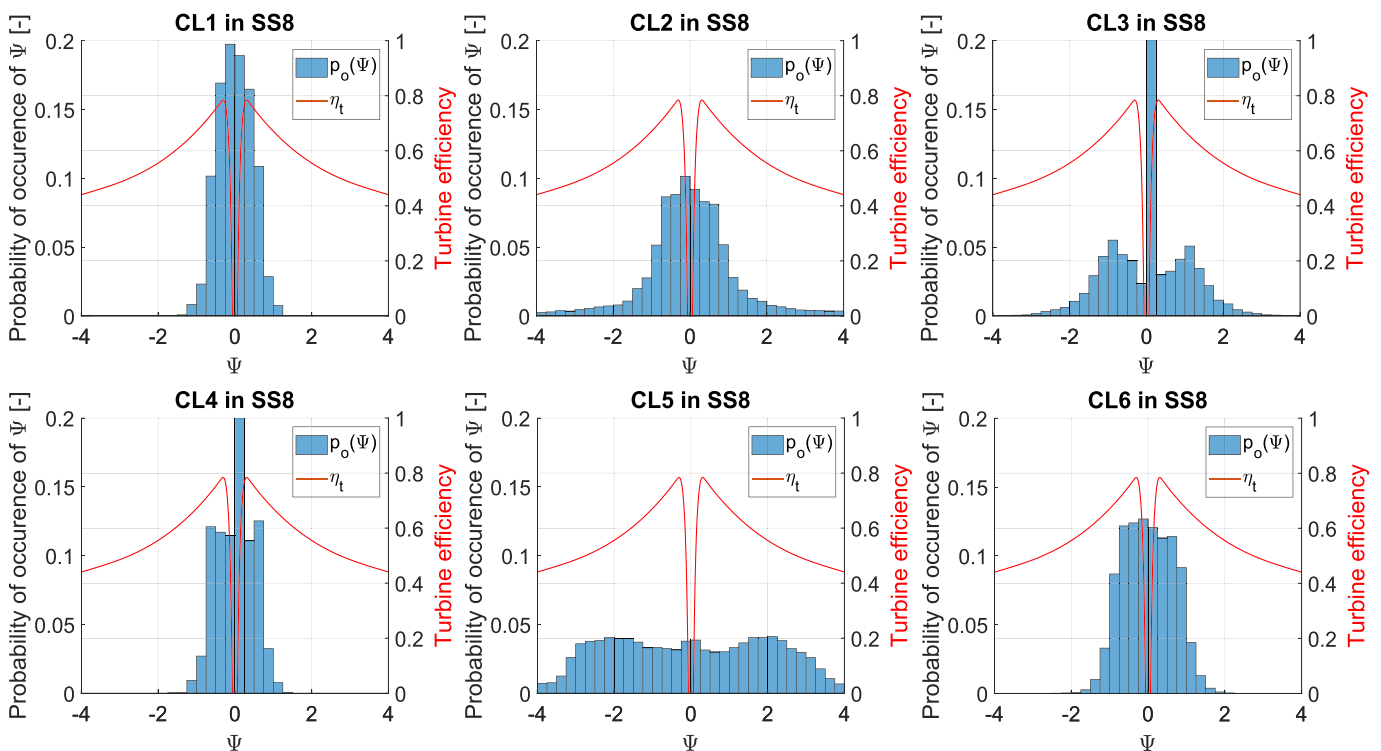

Fig. 7. Probability distribution of Ψ for the 6 CL during SS8.

overloading of the generator while all the others allow that kind of operation. During this SS, CL2 does not operate above twice the generator rated power. CL5 and CL6 are allowing operation until the maximal generator power. Also, referring to Fig. 8, CL1 and CL4 are the only two controllers that do not overload the generator during operation in SS10. CL2 and CL3 reach 1.5 times the generator rated power while CL6 operates the generator with peaks twice the nominal capacity, this value was elevated over 2.5 times in the case of CL5. The generator is able to operate in this configuration over its rated capacity as detailed in Section 2.3.5 but can produce an accelerated wear if exposed to that operation during a long time. In practice, if not properly ventilated the generator can generate an over-temperature. In the case the temperature rises over the one of the insulation class, the stator varnish protection can melt and the windings would produce a shortcut.

Fig. 10 gives an overall view of the power peaks produced by the different controllers. It shows a scatter plot of the peaks of power over the average electrical power — also known as peak-to-average power ratio — as a function of the average generator power for all CLs and all the SS. Control algorithms, such as CL5 or CL6, are the ones stressing the electrical components the most then followed by CL2 and CL3. This type of behaviour implies a poorer score regarding reliability issues and quality of power sent to the grid.

Focusing on the shut-off valve operation allows to assess how a CL relies on this component. The longer the valve is closed the higher the number of switching from open to closed position and the lower its life time. It is obvious the latching algorithms requires an intense operation of the valve and thus it is more likely to present a potential failure (c.f. Table 5). CL1 is also relying on the valve but for safety reason because the torque law, by avoiding generator overloads, allows the turbine to reach higher speeds, until reaching the cut-off speed that forces the valve to close. On the contrary CL2, CL5 and CL6 do not usually operate the safety valve because they allow higher torques to reduce the turbine speed.
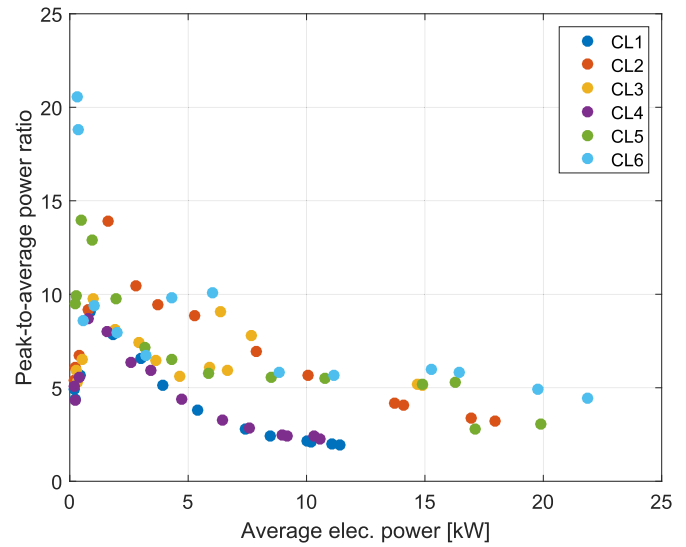

Fig. 10. Peak-to-average power in function of the average generator power each of CL for all the SS.

4.3. Highlights on simulation results

As a base case, CL1 is the reference law against which the other algorithms are tested. As an overall observation, its performance is fair and its philosophy is to set the turbine at its best operation point, which is achieved most of the time. It includes a peak-power control that prevent operating the generator higher than its nominal capacity. This type of operation, though the most careful considering generator reliability, have the effect to operate at higher speed lower torques. The impact is double, from one side there is less energy absorbed by the device because the safety valve
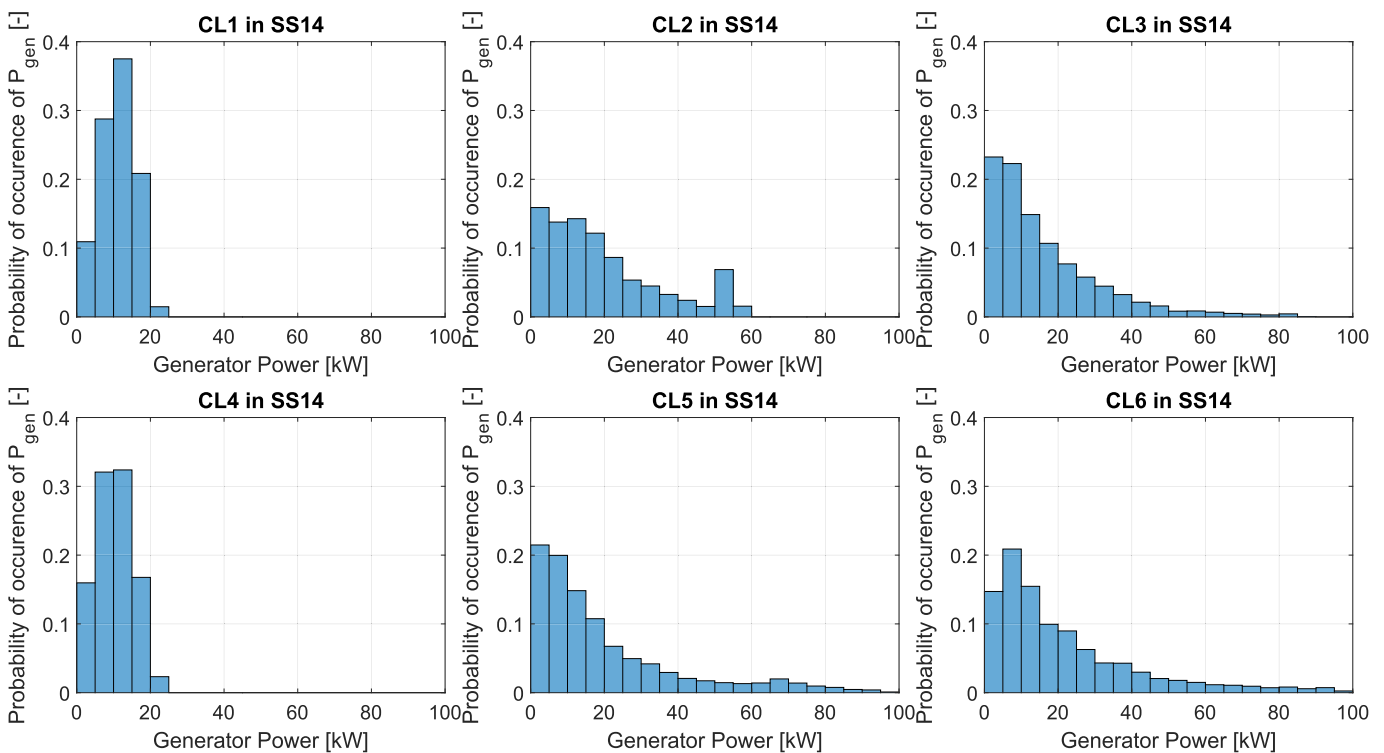

Fig. 9. Probability distribution of the electrical powers for the 6 CL during SS14.

Table 5
Turbine speed and valve actuation time for each CL in all SS.

SS	Average rotational speed [rad/s]						HSSV closed duration [s]					
	CL1	CL2	CL3	CL4	CL5	CL6	CL1	CL2	CL3	CL4	CL5	CL6
1	83	43	57	82	43	66	0	0	0	330	0	0
2	85	45	60	85	46	69	0	0	117	346	0	0
3	94	53	66	92	51	75	0	0	345	360	0	0
4	106	64	75	103	66	83	0	0	473	378	0	0
5	128	81	92	123	80	98	0	0	586	388	0	0
6	145	99	102	139	100	113	0	0	685	398	0	0
7	155	106	108	149	115	122	6	0	777	410	0	0
8	170	115	117	163	116	137	15	0	820	419	0	0
9	188	126	127	180	121	154	49	0	905	455	0	0
10	196	134	131	190	134	165	95	1	952	484	0	0
11	208	143	135	201	140	176	179	10	1036	549	0	4
12	210	141	126	203	138	176	196	21	1130	568	0	4
13	216	150	174	210	183	181	272	32	768	622	2	13
14	218	149	175	213	175	183	325	45	820	644	2	11

operates more often and on the other side the generator does not operated in optimal ranges. In what concerns Control Law 2, it is different from all the other control laws tested during simulations. CL2 relies strictly on the measured pressure within the plenum chamber to determine applied generator torque, while all other control laws presented here use turbine-generator speed to determine applied torque. The algorithm uses both a moving average pressure and the instantaneous chamber pressure. Due to the hysteresis in the OWC system, where changing pressure leads changing flow in the chamber, the application of the instantaneous pressure within the control law algorithm gives CL2 chronologic advantage over the other non-predictive control laws. This advantage manifests in the operations of the HSSV and the average rotational speed. However, the simulations show these advantages balanced by losses in both turbine and generator efficiency comparted to the other control laws. The annual energy production of CL2 is bested only by the reinforcement learning and the predictive control laws during simulation, this is largely due to an increase in available pneumatic power caused mostly by the minimal use of the HSSV. The limited use of the HSSV bodes well for the mechanical reliability of the OWC, but the peak-to-average generator power fluctuations could lead to electrical reliability degradation. The generator power fluctuations were unexpected as CL2 was originally designed to minimise swings in applied electrical torque, but the addition of the instantaneous pressure to the algorithm sacrificed electrical torque stability to moderate peaks in turbine rotational speed. These results highlight the delicate balance these control laws are attempting to maintain by maximising both mechanical and electrical performance. CL2 performs well, but there is room for improvement available.

In Control Law 3 and 4, the latching control laws are designed to maximise the hydrodynamic response of the OWC by adjusting the resonant frequency to match the frequency of the incoming waves. The latching system controls a valve that seals the plenum chamber of the OWC from outside atmosphere, which changes the hydro-dynamic properties of the system. During operation of CL3 and CL4, a secondary control law is required for the turbine-generator system. For the tests performed during these simulations, CL1 is applied to the turbine-generator. The results of the simulations show that they poorly operate in comparison to the other non-latching control laws, particularly in the higher energy sea states. Interestingly, CL3 produces more electrical energy than CL1 for SS 14, this is caused by better application of the HSSV. In SS 14, the latching of CL3 keeps the turbine speed lower, which increases the availability of the PTO system. There are several reasons for the poor performance of the latching algorithms. The main issue was

that hydrodynamic response of the Mutriku OWC Plant is relatively uniform across the various periods that affect the plant. This leaves little room for improving the response amplitude operator through latching, and when the latching valve is closed, the OWC converts zero pneumatic energy to mechanical energy. These losses are not recovered via hydrodynamic improvement. The larger energy sea states have longer periods, which lead to longer latching times and greater energy losses. The latching control theory behind the development of CL3 works best with two moving body WECs, but for the Mutriku plant, there is only one moving body. While the performance of CL3 and CL4 have proven poor during the Mutriku testing, there remains hope that it will be effective during offshore device testing.

Being an adaptive learning scheme and thus designed for long-term application, CL5 is reassuring that Reinforcement Learning achieves good performance (in comparison to the other CLs). Additionally, the CL converges to "optimal" control parameters after the set 12 h learning period, which gives evidence that the CL is allowing reasonable adaptation to changing conditions. In the context of adapting to changing systems parameters (e.g. changing physical parameters because of wear and tear of device components or adaptation to unforeseen environments), which highlights the main benefits of Reinforcement Learning driven control, the results are promising and could enable long-term management of optimal energy generation and power quality via scheduling of varying CLs.

The results obtained with the predictive algorithm CL6 have given evidence that good performance are due to consideration given to the overall PTO system, including both the turbine and the generator. Being predictive, it adapts as well to external and internal conditions during its receding horizon. It knows the profile of the incoming waves and is aware of the PTO components performance and limitations. Thus it optimally adapts to specific conditions and finds the best trade-off that optimises the control parameters. In the present analysis, the wave forecasting is ideal, meaning that the excitation force computed for the optimisation is the same as the one from the incoming waves that are hitting the plant. In practice the wave forecasting is not so straightforward to estimate. The quality of the optimisation is tied to the accuracy of the numerical model. This could also penalise the good performance in practical experiments at sea. By showing the best score in terms of electrical power production, CL6 has demonstrated it is the most promising among the other CL. Still this hypothesis is yet to be proved by tests in real sea conditions.

5. Test rig experiments

The proposed control algorithms need to pass a validation process before future real sea tests at Mutriku. The validation was performed in an electrical test infrastructure using Hardware-in-the-Loop (HIL) experiments. This step was considered to be indispensable to check the correct implementation of the controllers and gain confidence by repeated testing in a dry and controlled environment before any implementation at sea. The benefits of this kind of experimental testing are present in literature such as [70,71]. Two dry test labs were used for the experiments. From one side, the PTO test laboratory in Tecnalia to validate CL1, CL4 and CL6. On the other side, the PTO test rig of the MaREI Center, at University College of Cork, for validating CL2, CL3 and CL5.

5.1. Framework for the experiments

The idea of the HIL tests is to emulate the generator dynamic behaviour of one PTO system of the Mutriku power plant. As such, the WEC and turbine dynamics are simulated in real-time using a

dedicated computer, and an electric motor drives the generator with the computed turbine torque.

The used HIL infrastructure consists of two electrical machines facing each other, as described in Fig. 11. The hardware was divided into two key areas: the turbine side labelled as the emulated part and the generator side which is the real part. The turbine side is composed of a motor, that imposes the computed instantaneous turbine torque, the frequency converter, to control the motor, and the motor control software. These components aim to simulate the performance of the WEC and turbine under any sea condition. It is a simulation because the mathematical model is programmed in the motor control software so that it behaves like the OWC. The generator area includes the generator, the frequency converter to control the generator, and a Programmable Logic Controller (PLC) with the generator control software. This part represents the real equipment that is connected between the biradial turbine and the grid. The motor and the generator are coupled directly in the same shaft. The drive train is slowed down by the applied generator torque, and the new speed is sent to the emulation part of the model and thus closes the loop.

The most import aspect of this HIL configuration is that we remove Eq. (20) from a stand-alone numerical simulation. At each time-step of the simulation, the rotational speed of the motor/generator is measured instead of being computed. The measured rotational speed Ω and the computed pressure p uniquely define the turbine operating point Ψ. To guaranty the dynamic similarity of the experimental tests, the inertia of the HIL configuration (motor/generator) must respect inertia of the real turbine/generator set.

5.2. Scaling methodology

The laboratory infrastructure does not necessarily have the same physical characteristics of the PTO that is to be installed at Mutriku. The generator installed in the test benches have lower rated power than the one for the Mutriku power plant. The present work followed the methodology presented in Refs. [45,51,72,73] where the numerical model ran in-real time at prototype scale in a dedicated computer. The physical inputs and outputs of the numerical model were scaled down to control the motor/generator

(model scale) under similarity conditions with the turbine/generator set of the WEC PTO system (prototype scale).

Testbench drivetrains have losses that are different from the losses of the real PTO system. Losses cannot be scaled since they are an intrinsic property of the system. As such, it was decided to cancel the testbench losses by adding the torque losses to the reference torque computed in the numerical model that feeds the motor.

$$T_{t}^{m} = T_{t,ref}^{m} + T_{loss}, \tag{31}$$

where superscript m denotes model scale. The term T_{loss} was determined from free decay tests performed in the testbench.

5.3. Testbench results at Tecnalia

5.3.1. Description of the infrastructure

The characteristics of the electrical machines in the PTO Test laboratory are detailed in Table 6. Fig. 12 illustrates the infrastructure. The motor is controlled using a real-time simulation based on Matlab/Simulink environment and using an xPC configuration. This type of architecture is composed of a host PC for the development of the numerical model, a target PC operated by the Simulink Real-Time OS and where the model is downloaded and run in real time. A NI-6221 process board is installed in the target PC. It is the interface to manage the I/O. This setup simulates the performance of the WEC and turbine. The model includes the sea states and the WEC mathematical equations. It receives the turbine speed from

Table 6
Characteristics of both test rigs used for the experiments.

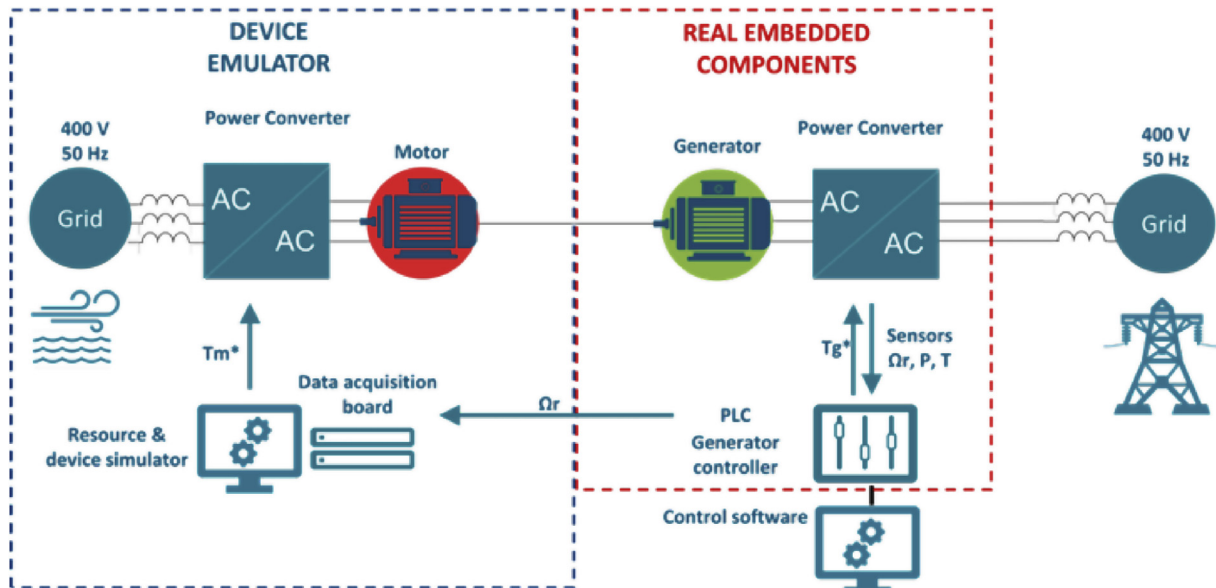|	Tecnalia		UCC	
	Motor	Gen.	Motor	Gen.
Type of generator	SCI	SCI	SCI	SCI
Rat. power [kW]	15	11	22	22
Nom. speed [rpm]	1460	768	1467	1472
Nb. pole-pairs	2	4	2	2
Frequency [Hz]	50	50	50	50
Rat. voltage [V]	400 Δ	400 Δ	400	400

*SCI: Squirrel cage induction.

Fig. 11. HIL testing framework.

Fig. 12. PTO Test lab at Tecnalia.

the test bench motor encoder and sends the torque that must be applied to the motor using the frequency converter. The motor frequency converter by Leroy-Somer is rated at 15 kW and allows peaks of power up to 28 kW. It can be controlled remotely via external 4/20 mA signals. Both speed and torque control modes are available. The generator is controlled with software programmed in a PLC from Beckhoff. The controller and the generator frequency converter are communicated through several analogical and digital inputs/outputs. In this way, the generator rotational speed is fed into the PLC. It is connected to a 400 V grid through a back-to-back bidirectional converter supplied by ABB. This converter is rated at 11 kW and allows flexible remote control of the generator torque or speed via analogical signals. In the current application, a torque reference is computed by the control law of the generator control software and applied by the frequency converter.

5.3.2. Validation evidence

Although several CL were tested in this infrastructure, the proof of validation is made for the predictive law CL6. The sea state SS7 was chosen to perform this test as it represents medium energy conditions for the Mutriku site. Fig. 13 shows curves of the rotational speed, turbine torque and generator power for both the numerical model simulations and the experimental results. Note that the experimental values are presented back to the prototype scale to be compared with the numerical simulation results. In that specific case for implementing CL6, an additional computer linked to the target PC was necessary to compute the predictive optimisation. The flow of data included, as input to the algorithm the state vector, including the test rig rotational speed, to initialise the system of equation. The outputs were the optimised control vector containing the new torque law parameters. The effects of the change is visible in the time series of the generator power with the sudden changes in the power profile. It is meant to set a harder torque law when a future set of waves arrives and softer when the waves are calmer.

5.4. Test lab results at UCC

5.4.1. Description of the infrastructure

The infrastructure used for the experimentation performed at the LiR National Ocean Test Facility at University College Cork is presented in Fig. 14. The basis of the UCC PTO test rig is described in detail in Ref. [74]. This test rig can be used to verify and evaluate

control laws, the reader is referred to Ref. [49].

Similar to the Tecnalia equipment, the UCC test rig is composed of two electrical machines directly coupled by a mechanical shaft, with a torque transducer between the two electrical machines. The mechanical drive shaft also includes a stainless steel flywheel that is connected to the system by a five-position gear box. The flywheel allows the drive shaft to be composed of one of five different inertial masses, which can be used to represent the inertia of the system to be tested. As described in Ref. [74], the generator rotor can be set to multiple configurations, depending on the system which is being emulated. The characteristics of the drive train is presented in Table 6.

The HIL interaction of the UCC test rig is controlled so that it is consistent with the operation of the Tecnalia test rig. The real-time simulation is carried out in a Matlab/Simulink environment with a host PC for development and a target PC for testing. The target PC interacts with a PLC that controls both drives and electrical machines of the test rig. The conditions modelled in software are relayed to the test bench equipment via available digital and analogue I/O. The torque applied to the motor acting as the system turbine is determined in the model and relayed to the PLC, while the rotational speed of the rotary system is fed from the PLC into the target PC and applied to the Simulink model in real time. When possible, the controller for the generator resides on the PLC and determines the generator braking torque. This will be done for testing of CL2 and CL3, but due to the complex nature of the computations required to apply the predictive nature of CL5, that controller will reside within the Simulink model and the generator braking torque will be sent to the PLC via the HIL system.

5.4.2. Validation evidence

The HIL tests that were carried out on the UCC test bench were compared to the results of the full simulations described in Section 4. This was done to ensure that the HIL tests and the link between the hardware and the real-time software model were operating correctly and accurately. An example of these comparisons is described and presented in this section. The selected example comes from testing carried out on CL2, where the controller existed within the PLC rather than the Simulink model. The same sea state as the one used in the CL6 validation in the other test rig is selected for the experiment. Fig. 15 shows plots of the rotational speed, applied turbine torque, and electrical power output for a 5-min period of testing for sea state 7. The model and test bench results show excellent agreement in system rotational speed and applied turbine torque. The test bench power is measured from the output of the grid side drive the back-to-back power converter, while the model power is estimated based on applied electrical braking torque and rotational speed, so although there is a visual discrepancy between to two, the average output power over the full simulation was similar. The validation techniques showed that the HIL testing represented the software model well, that the control laws could be accurately executed by a PLC controller, and that a model of the power electronics should be included in the Simulink model in the future.

6. Conclusion

In this paper, six different control algorithms were developed for the biradial using the Mutriku OWC plant. Most of the control strategies used a variable speed control framework while two added the concept of phase control by latching. Among the others, two controllers were adaptive controllers based on easily measurable data, one used artificial intelligence with a reinforcement learning scheme and the last one was a non-linear model predictive control. Simulation results of each controller for 14 irregular sea
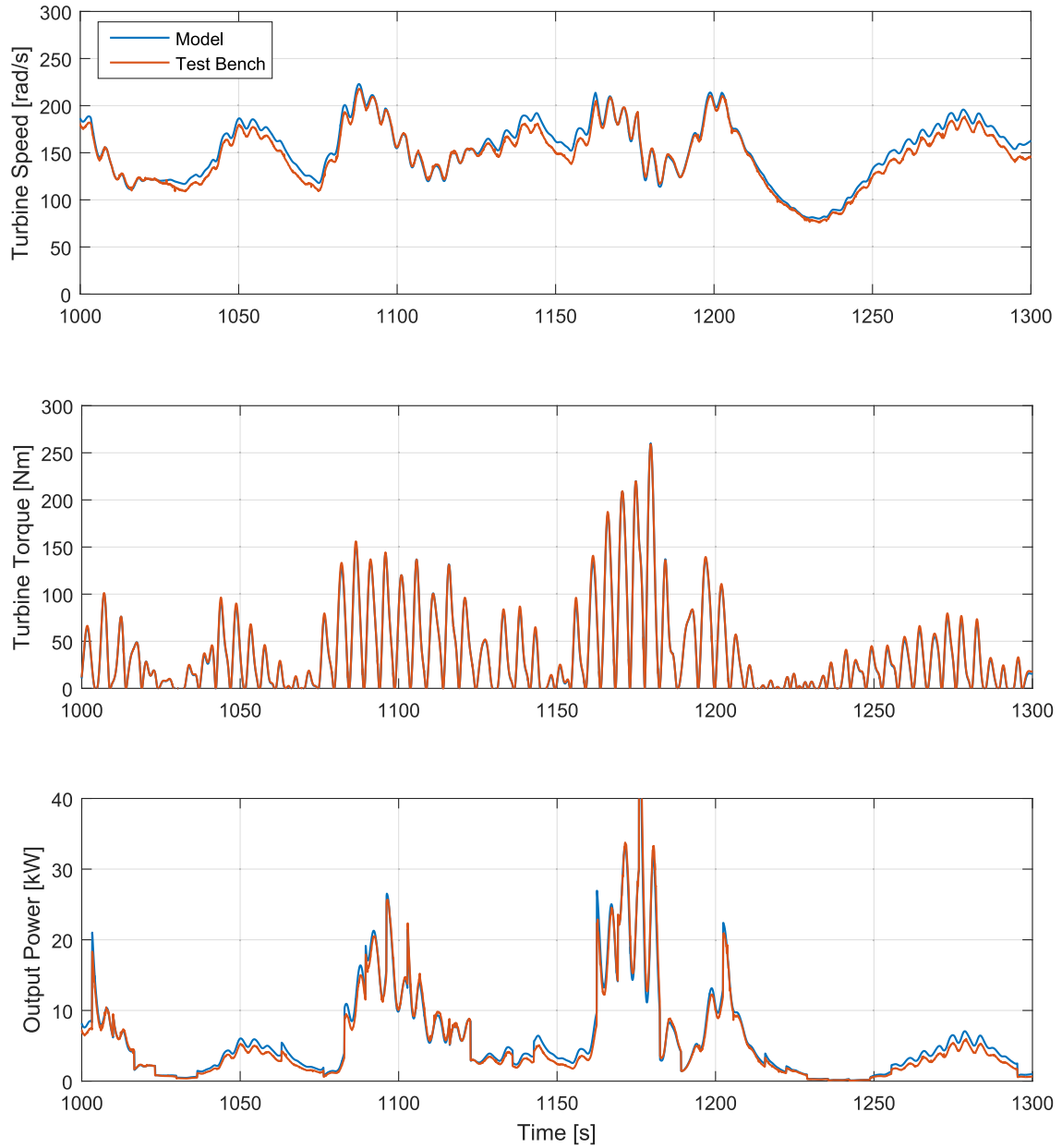
Fig. 13. Experimental results of CL6 validation on Tecnalia PTO test lab.
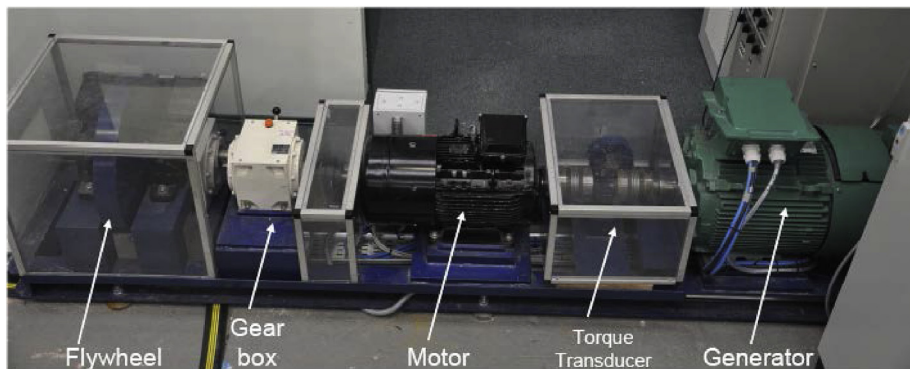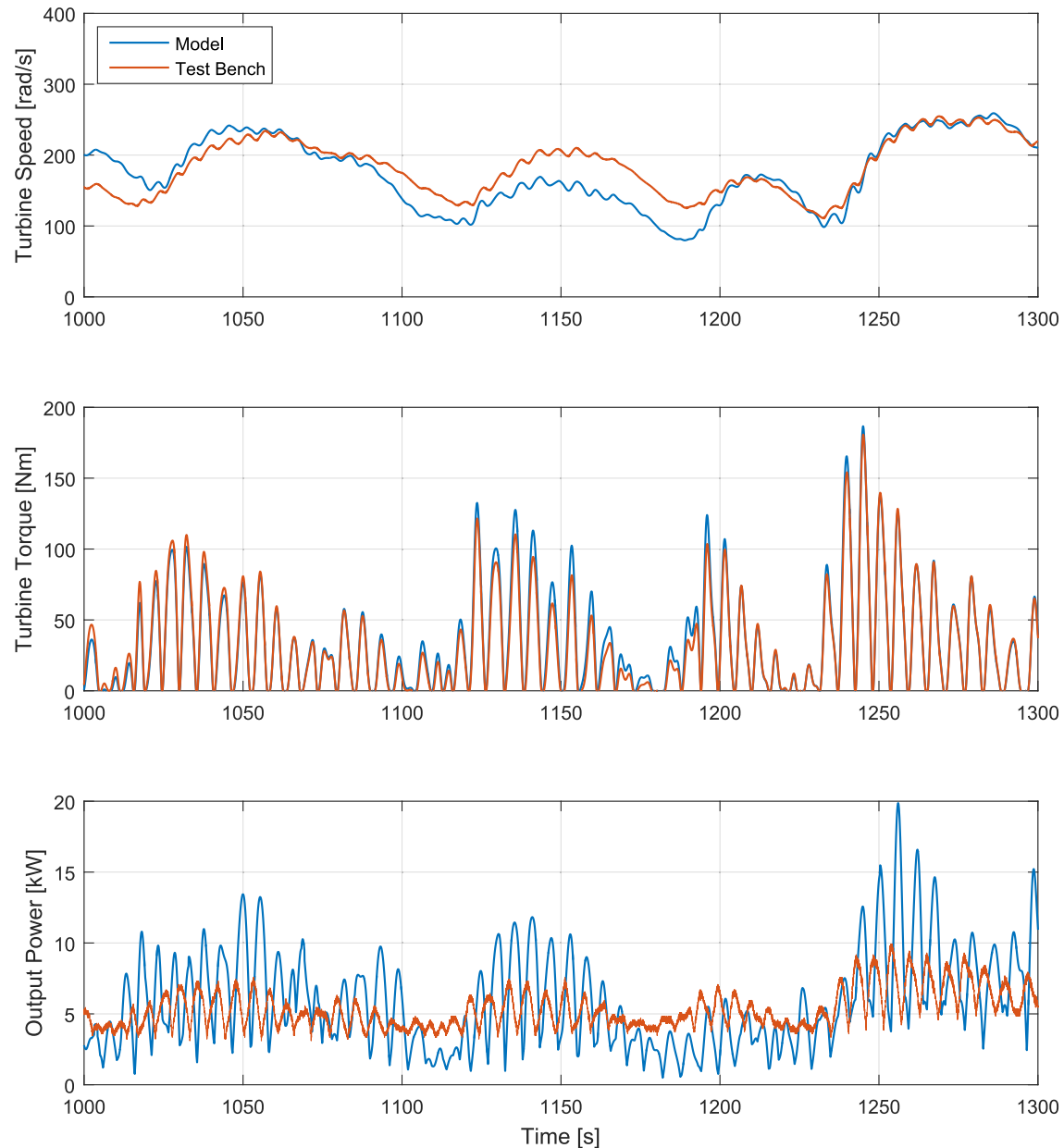

Fig. 14. PTO Test lab at UCC.

Fig. 15. Experimental results of CL2 validation on UCC PTO test bench.

states were proposed as evidence to support a comparative study of the controllers based on criteria such as performance and reliability. The latching controllers, though promising for floating devices, were found to be irrelevant in the specific case of Mutriku because the plant motion response did not allow to generate major improvements. The best performance were obtained by the more advanced controllers that are the reinforcement learning one and the MPC because they both included not only turbine efficiency into account but also included generator considerations in their optimisation process. No doubt an advantage of the RL is that it is a model-free controller. The MPC obtained the highest performance score in overall energy production, it outran the base case controller by over 20%, and showed in the best cases a total PTO efficiency close to 60%. These good results have to be contrasted by the fact that the wave forecasting for the online optimisation was

ideal as well as the plant model. In terms of reliability, the base case controller was the one inducing the least generator stresses because it included a peak-power control feature, avoiding generator overloads. This mode of operation forces the safety valve to operate more often and with it possible increase of failure rates. An Hardawre-In-the-Loop experimental phase was made on two electrical test rigs to validate the correct algorithms implementation, analyse their behaviour in a controlled dry environment and prepare for real sea deployment. Future work includes sea trials at the Mutriku OWC plant and will give the opportunity to challenge the hypothesis and outcomes of the present work to open sea results. In addition the future deployment at the plant will give the chance to adjust the Wave-to-Wire model with operational data and better predict the power production at the plant of future algorithms to be developed.

Appendix A. Wave amplitude attenuation function

Mutriku plant is situated shoreline, the waves when approaching the coast loses energy by friction with the sea bottom. To model the wave resource with linear wave theory, it would be incorrect to assume a typical wave spectrum for deep sea applications. In Ref. [75] the exploitable resource attenuation can be between 7 and 22% at a depth of 10 m. It is recommended to use a TMA spectrum to account for the water depth in wave modelling [76]. A TMA spectrum is a modification of a JONSWAP spectrum by including an attenuation function $\Upsilon(\omega, h)$ for a finite depth h.

$$S_{\text{TMA}}(\omega) = S_{\text{JS}}(\omega)\, \Upsilon(\omega, h). \tag{A.1}$$

Fig. A.16 represents several wave spectra using the JONSWAP spectrum and the TMA spectrum for the mean tidal depth at Mutriku, between 4.5 and 8.5 m depending on the tide. Another spectrum is added which represents waves measured by an ADCP installed by AZTI-Tecnalia in front of the plant wall. It appears clearly when comparing the two modelled spectra that they don't fit the one obtained locally. Instead, a custom Phi-function is created using the ADCP measurements for several sea states and comparing them with the JONSWAP ones modelled with the same H_s, T_e and peakedness γ. The attenuation coefficients for each frequency constitutes the curve in Fig. A.17.
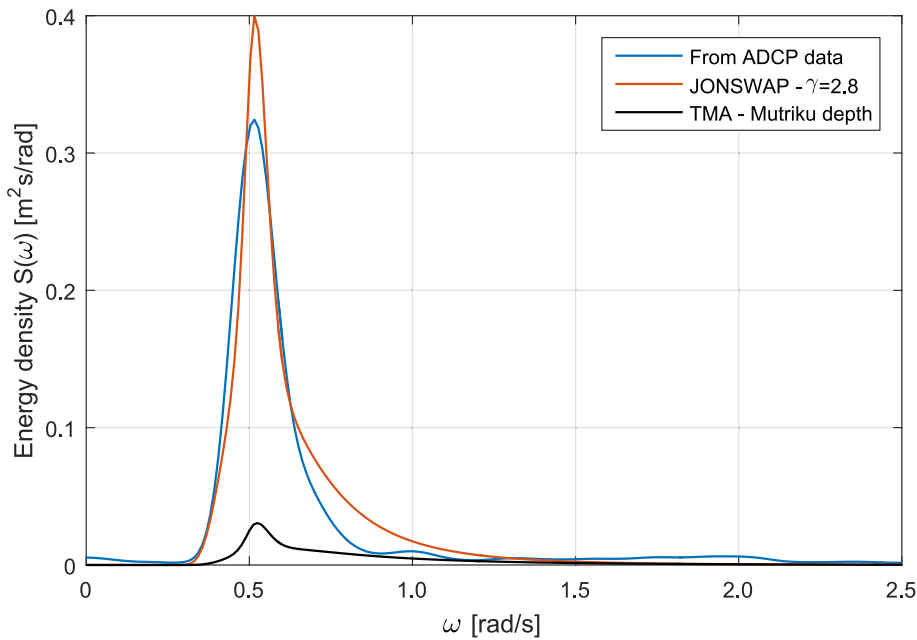

Figure A.16. Wave spectrum from ADCP measurement and different modelled spectra.
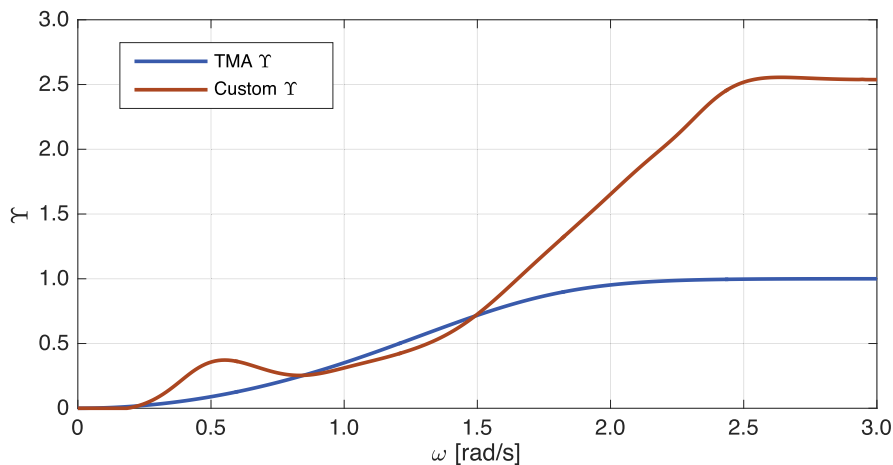

Figure A.17. Comparison of Υ-functions.

Appendix B. Supplementary data

Supplementary data to this article can be found online at https://doi.org/10.1016/j.renene.2019.08.074.

References

[1] Eurostat, Renewable Energy in the EU - Share of Renewables in Energy Consumption in the EU Reached 17% in 2016, Jan. 2018.
[2] IRENA, Renewable Energy Statistics 2018, The International Renewable Energy Agency, Abu Dhabi, 2018. ISBN 978-92-9260-077-8, https://www.irena.org/-/media/Files/IRENA/Agency/Publication/2018/Jul/IRENA_Renewable_Energy_Statistics_2018.pdf.
[3] T.W. Thorpe, An overview of wave energy technologies: status, performance and costs. Tech. Rep., ETSU, 1999.
[4] B. Drew, A. Plummer, M.N. Sahinkaya, A review of wave energy converter technology, Journal of Power and Energy 223 (2009) 887—902, https://doi.org/10.1243/09576509JPE782.
[5] A.F.D.O. Falcão, Wave energy utilization: a review of the technologies, Renew. Sustain. Energy Rev. 14 (3) (2010) 899—918, https://doi.org/10.1016/j.rser.2009.11.003.
[6] A. Babarit, A database of capture width ratio of wave energy converters, Renew. Energy 80 (2015) 610—628, https://doi.org/10.1016/j.renene.2015.02.049.
[7] I. López, J. Andreu, S. Ceballos, I. Martínez de Alegría, I. Kortabarria, Review of wave energy technologies and the necessary power-equipment, Renew. Sustain. Energy Rev. 27 (2013-11) 413—434, https://doi.org/10.1016/j.rser.2013.07.009.
[8] J. Grimwade, D. Hails, E. Robles, F. Salcedo, J. Bard, P. Kracht, J.-B. Richard, A.R. Årdal, J.I. Marvik, N.A. Ringheim, H. Svendsen, M. Molinas, MARINET Deliverable 2.3 - Review of Relevant PTO Systems, NAREC; TECNALIA; FH-IWES; SINTEF;NTNU, 2012. Tech. rep.
[9] Y. Lin, J. Bao, H. Liu, W. Li, L. Tu, D. Zhang, Review of hydraulic transmission technologies for wave power generation, Renew. Sustain. Energy Rev. 50 (2015) 194—203, https://doi.org/10.1016/j.rser.2015.04.141.
[10] A. Têtu, Chapter 8 - power-take-off systems for WECs, in: A. Pecher, J.P. Kofoed (Eds.), Handbook of Ocean Wave Energy, Springer, 2016, pp. 203—220, https://doi.org/10.1007/978-3-319-39889-1.
[11] T.V. Heath, A review of oscillating water columns, Philos. Trans. R. Soc. A Math. Phys. Eng. Sci. 370 (1959) (2012) 235—245, https://doi.org/10.1098/rsta.2011.0164.
[12] N. Delmonte, D. Barater, F. Giuliani, P. Cova, G. Buticchi, Review of oscillating water column converters, IEEE Trans. Ind. Appl. (2015), https://doi.org/10.1109/TIA.2015.2490629, 1—1.
[13] A.F.O. Falcão, J.C.C. Henriques, Oscillating-water-column wave energy converters and air turbines: a review, Renew. Energy 85 (2016) 1391—1424, https://doi.org/10.1016/j.renene.2015.07.086.
[14] J.P. Kofoed, The wave energy sector, in: A. Pecher, J.P. Kofoed (Eds.), Handbook of Ocean Wave Energy, vol. 7, Springer International Publishing, 2017, pp. 17—42, https://doi.org/10.1007/978-3-319-39889-1_2.
[15] A.F.O. Falcão, L.M.C. Gato, The pico OWC wave power plant: its life from conception to closure 1986 2018, in: Renew 2018, Advances in Renewable Energies Offshore Guedes Soares, 2019, p. 9.
[16] D.L. Bull, M.E. Ochs, Technological cost-reduction pathways for oscillating water column wave energy converters in the marine hydrokinetic environment, Tech. Rep. SAND2013—7205 (2013-09-01) 1092997, https://doi.org/10.2172/1092997.
[17] J. Falnes, Optimum control of oscillation of wave-energy converters, Int. J. Offshore Polar Eng. Vol. 12, No. 2,.
[18] J. Ringwood, S. Simani, Overview of modelling and control strategies for wind turbines and wave energy devices: comparisons and contrasts, Annu. Rev. Contr. 40 (2015) 27—49, https://doi.org/10.1016/j.arcontrol.2015.09.003.
[19] G. Bacelli, Optimal control of wave energy converters, IEEE Transaction on Sustainable Energy 6 (2) (2015) 294—302, https://doi.org/10.1109/TSTE.2014.2371536.
[20] L. Wang, J. Isberg, E. Tedeschi, Review of control strategies for wave energy conversion systems and their validation: the wave-to-wire approach, Renew. Sustain. Energy Rev. 81 (2018-01) 366—379, https://doi.org/10.1016/j.rser.2017.06.074.
[21] J. Falnes, Optimum control of oscillation of wave-energy converters, in: Eleventh International Offshore and Polar Engineering Conference, vol. I, Stavanger, Norway, 2001, pp. 567—574.
[22] J. Falnes, T. Bjarte-Larsson, Theoretical and experimental investigation of wave energy conversion by a phase-controlled heaving body, Proceedings of the Institution of Mechanical Engineers, Part M, Journal of Engineering for the Maritime Environment 220 (4) (2006) 175—183, https://doi.org/10.1243/14750902JEME52.
[23] J. Hals, J. Falnes, T. Moan, A comparison of selected strategies for adaptive control of wave energy converters, J. Offshore Mech. Arct. Eng. 133 (3) (2011), 031101, https://doi.org/10.1115/1.4002735.
[24] A. Babarit, G. Duclos, A.H.A.H. Clément, Comparison of latching control strategies for a heaving wave energy device in random sea, Appl. Ocean Res. 26 (5) (2004) 227—238, https://doi.org/10.1016/j.apor.2005.05.003.
[25] A. Babarit, A.H. Clément, Optimal latching control of a wave energy device in regular and irregular waves, Appl. Ocean Res. 28 (2) (2006) 77—91, https://doi.org/10.1016/j.apor.2006.05.002.
[26] W. Sheng, R. Alcorn, A. Lewis, On improving wave energy conversion, part II: development of latching control technologies, Renew. Energy 75 (2015), https://doi.org/10.1016/j.renene.2014.09.049.
[27] J. Hals, J. Falnes, T. Moan, Constrained optimal control of a heaving buoy wave energy converter, J. Offshore Mech. Arct. Eng. 133 (3) (2011) 31101, https://doi.org/10.1115/1.4001431.
[28] G. Li, M.R. Belmont, Model predictive control of sea wave energy converters — Part I: a convex approach for the case of a single device, Energy 69 (Guang Li) (2014) 453—463, https://doi.org/10.1016/j.renene.2014.03.070.
[29] N. Faedo, S. Olaya, J. V. Ringwood, Optimal control, MPC and MPC-like algorithms for wave energy systems: an overview, IFAC Journal of Systems and Controldoi:10.1016/j.ifacsc.2017.07.001.
[30] A.S. Zurkinden, F. Ferri, S. Beatty, J.P. Kofoed, M.M. Kramer, Non-linear numerical modeling and experimental testing of a point absorber wave energy converter, Ocean. Eng. 78 (2014) 11—21, https://doi.org/10.1016/j.oceaneng.2013.12.009. January 2016.
[31] J.A.M. Cretel, A.W. Lewis, G.P. Thomas, G. Lightbody, A Critical assessment of latching as control strategy for wave-energy point absorbers, in: Twenty First International Society of Offshore and Polar Engineers Conference, Maui, HA, USA, vol. 8, 2011, pp. 680—686.
[32] J. Sjolte, C.M. Sandvik, E. Tedeschi, M. Molinas, Exploring the potential for increased production from the wave energy converter lifesaver by reactive control, Energies 6 (8) (2013), https://doi.org/10.3390/en6083706.
[33] F. Fusco, J.V. Ringwood, A study of the prediction requirements in real-time control of wave energy converters, IEEE Transactions on Sustainable Energy 3 (1) (2012) 176—184, https://doi.org/10.1109/TSTE.2011.2170226.
[34] M. Lopes, J. Hals, R. Gomes, T. Moan, L. Gato, A.O. Falcão, Experimental and numerical investigation of non-predictive phase-control strategies for a point-absorbing wave energy converter, Ocean. Eng. 36 (5) (2009-04) 386—402, https://doi.org/10.1016/j.oceaneng.2009.01.015.
[35] J. Wu, Y. Yao, L. Zhou, M. Göteman, Real-time latching control strategies for the solo duck wave energy converter in irregular waves, Appl. Energy 222 (2018-07) 717—728, https://doi.org/10.1016/j.apenergy.2018.04.033.
[36] Quoceant Ltd, Power Take-off: Non-confidential Summary Report, 2016.
[37] A. Falcao, Control of an oscillating-water-column wave power plant for maximum energy production, Appl. Ocean Res. 24 (2002) 73—82.
[38] F.-X. Faÿ, J.C. Henriques, M. Marcos, E. Robles, Review of control strategies for oscillating water column wave energy converters, in: 11th European Wave and Tidal Energy Conference, Nantes, France, Nantes, France, 2015, https://doi.org/10.3723/ut.32.003, 10A3—3—1.
[39] A. Falcão, J. Henriques, L. Gato, Rotational speed control and electrical rated power of an oscillating-water-column wave energy converter, Energy (2017), https://doi.org/10.1016/j.energy.2016.11.078.
[40] J. Henriques, W. Sheng, A.F.O. Falcao, L.M.C. Gato, A comparison of biradial and wells air turbines on the mutriku breakwater OWC wave power plant, in: 32nd International Conference on Ocean, Offshore and Arctic Engineering, 2017.
[41] A.d.O. Falcao, P.A.P. Justino, OWC wave energy devices with air flow control, Ocean. Eng. 26 (12) (1999) 1275—1295.
[42] J. Lekube, A. Garrido, I. Garrido, E. Otaola, J. Maseda, Flow control in wells turbines for harnessing maximum wave power, Sensors 18 (2) (2018-02-10) 535, https://doi.org/10.3390/s18020535.
[43] J.C.C. Henriques, A.F.O. Falcão, R.P.F. Gomes, L.M.C. Gato, Latching control of an OWC spar-buoy wave energy converter in regular waves, in: ASME 2012 31st International Conference on Ocean, Offshore and Arctic Engineering, American Society of Mechanical Engineers, 2012, pp. 641—650.
[44] J.C. Henriques, J.C. Chong, A.F. Falcão, R.P. Gomes, Latching control of a floating oscillating water column wave energy converter in irregular waves, in: ASME 2014 33rd International Conference on Ocean, Offshore and Arctic Engineering, American Society of Mechanical Engineers, 2014. V09AT09A017—V09AT09A017.
[45] J. Henriques, L. Gato, A. Falcão, E. Robles, F.-X. Faÿ, Latching control of a floating oscillating-water-column wave energy converter, Renew. Energy 90 (2016-05) 229—241, https://doi.org/10.1016/j.renene.2015.12.065.
[46] J.a.C. Henriques, J.a.M. Lemos, L. Eça, L.M. Gato, A.F. Falcão, A high-order discontinuous galerkin method with mesh refinement for optimal control, Automatica 85 (2017-11) 70—82, https://doi.org/10.1016/j.automatica.2017.07.029.
[47] F.-X. Faÿ, M. Marcos, E. Robles, Novel predictive latching control for an oscillating water column buoy, in: Proceedings of the 12th European Wave and Tidal Energy Conference, Cork, Ireland, 2017, p. 819.
[48] M.F.P. Lopes, J. Hals, R.P.F. Gomes, T. Moan, L.M.C. Gato, A.F.d.O. Falcão, Experimental and numerical investigation of non-predictive phase-control strategies for a point-absorbing wave energy converter, Ocean. Eng. 36 (5) (2009), https://doi.org/10.1016/j.oceaneng.2009.01.015.
[49] S. Ceballos, J. Rea, I. Lopez, J. Pou, E. Robles, D.L. O'Sullivan, Efficiency optimization in low inertia wells turbine-oscillating water column devices, IEEE Trans. Energy Convers. 28 (3) (2013) 553—564, https://doi.org/10.1109/TEC.2013.2265172.
[50] S. Armstrong, J. Rea, F.-X. Faÿ, E. Robles, Lessons learned using electrical research test infrastructures to address the electrical challenges faced by ocean energy developers, International Journal of Marine Energy 12 (2015-12)

46–62, https://doi.org/10.1016/j.ijome.2015.08.004.

[51] J. Henriques, R. Gomes, L. Gato, A. Falcão, E. Robles, S. Ceballos, Testing and control of a power take-off system for an oscillating-water-column wave energy converter, Renew. Energy 85 (2016-01) 714–724, https://doi.org/10.1016/j.renene.2015.07.015.

[52] F.-X. Faÿ, E. Robles, J. Henriques, M. Marcos, Best practices for the use of electrical test infrastructures to validate control strategies: a case study in wave energy conversion, in: Renew 2016 2nd International Conference on Renewable Energies Offshore, 2016-10, p. 445.

[53] J. Lavelle, J.P. Kofoed, Power Production Analysis of the Oe Buoy Wec for the Cores Project, Department of Civil Engineering, Aalborg University, 2011. Tech. rep.

[54] F. Thiebaut, P. DO'Sullivan, S. Ceballos, J. López, C. Boake, J. Bard, N. Brinquete, J. Varandas, L.M.C. Gato, R. Alcorn, in: Proceedings of the 9th European Wave and Tidal Energy Conference, Southampton, UK, 2011.

[55] K. Monk, D. Conley, M. Lopes, Q. Zou, Pneumatic power regulation by wave forecasting and real-time relief valve control for an OWC, in: European Wave and Tidal Conference, Aalborg, Denmark, 2013.

[56] K. Monk, V. Winands, M. Lopes, Chamber pressure skewness corrections using a passive relief valve system at the Pico oscillating water column wave energy plant, Renew. Energy (2018), https://doi.org/10.1016/j.renene.2018.04.037.

[57] Y. Torre-Enciso, I. Ortubia, L.I. de Aguileta, J. Marqués, I.L. de Aguileta, J. Marqués, Mutriku wave power plant: from the thinking out to the reality, in: Proc 8th European Wave Tidal Energy Conf, Uppsala, Sweden, 2009, pp. 319–329.

[58] W.K. Tease, J. Lees, A. Hall, Advances in oscillating water column air turbine development, in: Proc. of the Seventh European Wave and Tidal Energy Conference, Porto, Portugal, 2007.

[59] F.-X. Faÿ, J. Kelly, J. Henriques, A. Pujana, M. Abusara, M. Mueller, I. Touzon, P. Ruiz-Minguela, Numerical simulation of control strategies at mutriku wave power plant, in: ASME 2018 37th International Conference on Ocean, Offshore and Arctic Engineering, vols. 17–22, 2018, p. 11. June 2018, Madrid, Spain.

[60] DNV-RP-c205: Environmental Conditions and Environmental Loads, (Tech. rep)..

[61] G. Duclos, A.H. Clément, G. Chatry, Absorption of outgoing waves in a numerical wave tank using a self-adaptive boundary condition, Int. J. Offshore Polar Eng. 11 (03) (2001) 8.

[62] Abb Catalogue. 'low Voltage General Purpose Motors, 2004 accessed: 2018-08-15.

[63] S.m. muyeen, Wind Energy Conversion Systems, springer verlag london limited, 2012.

[64] D. Wang, K. Lu, Energy Storage Systems, Sdwed D3, vol. 1, 2013.

[65] Ak Steel, 'selection of Electrical Steels for Magnetic Cores, 2007 accessed: 2018-08-16.

[66] A.d.O. Falcão, O. De, The shoreline OWC wave power plant at the azores, in: Fourth European Wave Energy Conference, Aalborg, Denmark, Dec, 2000, pp. 4–6.

[67] W. Sheng, R. Alcorn, A. Lewis, On improving wave energy conversion, part i: optimal and control technologies, Renew. Energy 75 (2015-03) 922–934, https://doi.org/10.1016/j.renene.2014.09.048.

[68] W. Sheng, R. Alcorn, A. Lewis, On improving wave energy conversion, part II: development of latching control technologies, Renew. Energy 75 (2015-03) 935–944, https://doi.org/10.1016/j.renene.2014.09.049.

[69] E. Anderlini, D.I.M. Forehand, P. Stansell, Q. Xiao, M. Abusara, Control of a point absorber using reinforcement learning, IEEE Transactions on Sustainable Energy 7 (4) (2016) 1681–1690, https://doi.org/10.1109/TSTE.2016.2568754.

[70] S. Armstrong, J. Rea, F.-X. Faÿ, E. Robles, Lessons learned using electrical research test infrastructures to address the electrical challenges faced by ocean energy developers, International Journal of Marine Energy 12 (2015-12) 46–62, https://doi.org/10.1016/j.ijome.2015.08.004.

[71] F.X. Faÿ, E. Robles, J.C. Henriques, M. Marcos, Best practises for the use of electrical test infrastructures to validate control strategies: a case study in wave energy conversion, in: Second International Conference on Renewable Energies Offshore, Lisboa, Portugal, 2016, pp. 445–452.

[72] S. Ceballos, J. Rea, E. Robles, I. Lopez, J. Pou, D. O'Sullivan, Control strategies for combining local energy storage with wells turbine oscillating water column devices, Renew. Energy 83 (2015) 1097–1109, https://doi.org/10.1016/j.renene.2015.03.030.

[73] J. Henriques, L. Gato, J. Lemos, R. Gomes, A. Falcão, Peak-power control of a grid-integrated oscillating water column wave energy converter, Energy 109 (2016) 378–390, https://doi.org/10.1016/j.energy.2016.04.098.

[74] J. Rea, J. Kelly, R. Alcorn, D. O'Sullivan, Development and operation of a power take off rig for ocean energy research and testing, in: Eur. Wave Tidal Energy Conf., Southampton, UK, 2011.

[75] M. Folley, T. Whittaker, Analysis of the nearshore wave energy resource, Renew. Energy 34 (7) (2009) 1709–1715, https://doi.org/10.1016/j.renene.2009.01.003.

[76] DNV-RP-F205, Global Performance Analysis of Deepwater Floating Structures, Det Norske Veritas, 2010.